River delta morphotypes emerge from multiscale characterization of shorelines

Lawrence Vulis[1], Alejandro Tejedor[2], Hongbo Ma[3], Jaap H Nienhuis[4], Connor Broaddus[1], Jack Brown[5], Douglas Arthur Edmonds[6], Joel Carey Rowland[7], and Efi Foufoula-Georgiou[1]

[1]University of California, Irvine
[2]Paris-Sorbonne University Abu Dhabi
[3]Tsinghua University
[4]Utrecht University
[5]Indiana University,
[6]Indiana University
[7]Los Alamos National Laboratory (DOE)

January 17, 2023

Abstract

Delta shoreline structure has long been hypothesized to encode information on the relative influence of fluvial, wave, and tidal processes on delta formation and evolution. We introduce here a novel multiscale characterization of shorelines by defining three process-informed morphological metrics. We show that this characterization yields self-emerging classes of morphologically similar deltas, i.e., delta morphotypes, and also predicts the dominant forcing of each morphotype. Then we show that the dominant forcings inferred from shoreline structure generally align with those estimated via relative sediment fluxes, while positing that misalignments arise from spatiotemporal heterogeneity in deltaic sediment fluxes not captured in their estimates. The proposed framework for shoreline characterization advances our quantitative understanding of how shoreline features reflect delta forcings, and may aid in deciphering paleoclimate from images of ancient deposits and projecting delta morphologic response to changes in sediment fluxes.

River delta morphotypes emerge from multiscale characterization of shorelines

L. Vulis[1,2], A. Tejedor[3,1], H. Ma[4,1], J. H. Nienhuis[5], C. M. Broaddus[1], J. Brown[6], D. A. Edmonds[6], J. C. Rowland[2], and E. Foufoula-Georgiou[1,7]

[1]Department of Civil and Environmental Engineering, University of California Irvine,
[2]Earth and Environmental Sciences Division, Los Alamos National Laboratory
[3]Department of Science and Engineering, Sorbonne University Abu Dhabi
[4]State Key Laboratory of Hydroscience and Engineering, Tsinghua University
[5]Department of Physical Geography, Utrecht University
[6]Department of Earth and Atmospheric Sciences, Indiana University
[7]Department of Earth System Science, University of California Irvine

Keypoints

1. Three process-informed, geometric, and spectral metrics are introduced to characterize multiscale shoreline features
2. Unsupervised clustering of the shoreline metrics reveals 5 distinct delta morphotypes which correspond to distinct forcings
3. Morphotypes can be robustly estimated from readily available satellite imagery

Abstract

Delta shoreline structure has long been hypothesized to encode information on the relative influence of fluvial, wave, and tidal processes on delta formation and evolution. We introduce here a novel multiscale characterization of shorelines by defining three process-informed morphological metrics. We show that this characterization yields self-emerging classes of morphologically similar deltas, i.e., delta morphotypes, and also predicts the dominant forcing of each morphotype. Then we show that the dominant forcings inferred from shoreline structure generally align with those estimated via relative sediment fluxes, while positing that misalignments arise from spatiotemporal heterogeneity in deltaic sediment fluxes not captured in their estimates. The proposed framework for shoreline characterization advances our quantitative understanding of how shoreline features reflect delta forcings, and may aid in deciphering paleoclimate from images of ancient deposits and projecting delta morphologic response to changes in sediment fluxes.

Plain Language Summary

It has long been posited that the observed diversity in the shapes of river deltas reflects the relative strength of river, wave, and tide forcings acting on the delta. However, rigorous quantification of delta morphology and how it relates to forcing is still lacking. Here we introduce a new multiscale geometric framework which characterizes river delta morphology via measures of its shoreline structure and then use these measures to first separate deltas into morphological classes called morphotypes and second to infer the dominant forcing of each morphotype. We then show that the dominant forcings revealed by delta shoreline structure generally align with quantitative estimates of the relative amount of sediment transported by each forcing, and posit that misalignments may reflect space-time heterogeneities in the sediment transport rates not captured in their estimated values. The proposed framework enables easy and quantifiable delta classification based on readily-available remote sensing images and may yield insight into predicting deltaic geomorphic response to changing forcings.

Introduction:

River deltas are complex ecogeomorphic landscapes which are home to upwards of 300 million people due to their fertile soils and rich ecosystems (Edmonds et al., 2020). Their intricate hydromorphology controls nearshore biogeochemical function (Knights et al., 2020; Zoccarato et al., 2019), connectivity between surface and subsurface hydrogeology and reservoirs (Sawyer et al., 2015), coastal resilience (Hoitink et al., 2020; Tognin et al., 2021), and ecosystem services (Adams et al., 2018). Deltas are particularly vulnerable to climate change due to their low relief, coastal proximity, and large populations (Edmonds et al., 2020; Hoitink et al., 2020). It is therefore critical to understand how sea level rise and changing riverine sediment loads will impact these systems (Chadwick et al., 2020; Nienhuis et al., 2023) and towards this goal, developing a

quantitative framework which links the driving forces forming deltas to delta morphology and function is imperative.

Fifty years ago, Galloway introduced the paradigm that river deltas are shaped by the interplay of progradational riverine forcings and erosional marine (wave and tide) forcings, which has steered subsequent research on river delta evolution (Galloway, 1975; see also e.g. (Ainsworth et al., 2011; Anthony, 2015; Bhattacharya & Giosan, 2003; Nienhuis et al., 2020; Seybold et al., 2007; Syvitski & Saito, 2007). The relative balance of these forcings and the multiple spatio-temporal scales at which they operate result in a stunning degree of variability in shoreline structure and channel network geometry and topology (Fagherazzi et al., 2015; Hoitink et al., 2017; Jerolmack & Swenson, 2007; Konkol et al., 2022; Tejedor et al., 2016, 2017). Rivers act to prograde the delta planform at large scales and increase roughness at fine scales via the growth of mouth bars and distributary channel expansion (Fagherazzi et al., 2015; Wolinsky et al., 2010). Waves generate alongshore transport that diffuse sediment along the shoreline at fine scales but can lead to spits at coarser scales (Ashton & Giosan, 2011) and suppress mouth-bar development (Jerolmack & Swenson, 2007). Tidal forces widen distributary channels and construct headless channels which lack connections to the upstream river, roughening the shoreline at multiple scales (Hoitink et al., 2017; Nienhuis et al., 2018).

Recently, the relative magnitudes of the forcings in the Galloway framework have been quantified via a sediment flux approach (Nienhuis et al., 2020). However, shoreline shape, a crucial ingredient in the qualitative morphological classification originally posed by Galloway (See Table 2; (Galloway, 1975), has not been quantified in a way to differentiate between visually distinct deltas, nor has been shown to have a clear relationship with forcings, e.g. (Baumgardner, 2016). This is in part because analysis of shoreline structure has typically focused on a single length scale using

metrics such as shoreline variability (Straub et al., 2015) roughness or rugosity measures (Baumgardner, 2016; Caldwell & Edmonds, 2014; Geleynse et al., 2012), and shape factors (Lauzon et al., 2019; Nienhuis et al., 2015; Wolinsky et al., 2010). Such metrics do not necessarily measure shoreline structure at process length scales, nor do they capture the multiscale variability caused by the interplay of the three driving forces.

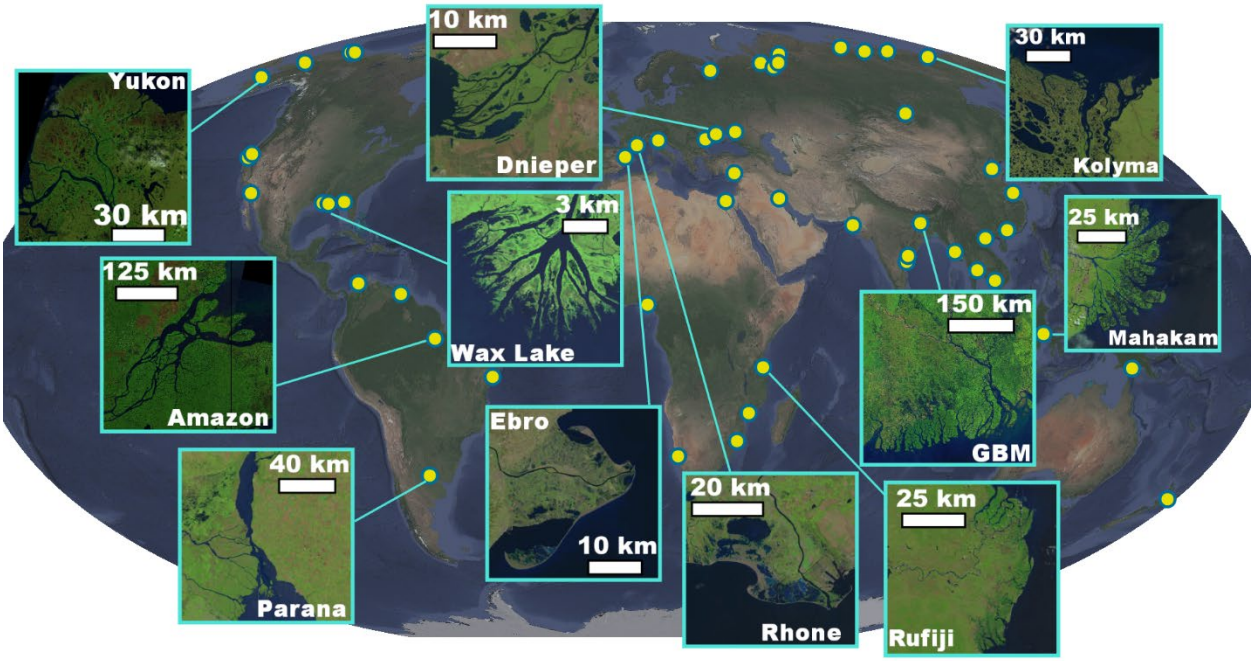

Figure 1. The morphologic variability of Earth's deltas. River deltas show differences in shoreline structure attributed to the relative balance of river, wave, and tidal sediment fluxes (Galloway, 1975). Yellow dots show locations of a globally distributed sample of 54 deltas analyzed in this study. Satellite imagery courtesy of Landsat and Google Earth.

Here, we propose a set of process-informed, multiscale metrics of river delta shoreline shape which combine geometric and spectral measures to develop a quantitative classification of delta morphology. Our approach utilizes localized analysis of shoreline structure both in space and wavenumber domains to isolate features corresponding to different processes acting at multiple scales. Unsupervised clustering of the shoreline morphometrics identifies five classes of

morphologically similar deltas, i.e. delta morphotypes. Based on the values of the process-informed metrics, dominant forcings are attributed to each morphotype, which we then show to generally align with the dominant forcings quantitatively estimated by their relative sediment fluxes (Supplementary Material; Nienhuis et al., 2020). We hypothesize that misalignments between the two are due to spatiotemporal heterogeneity in the sediment fluxes which are not captured by their estimated values. The novel shoreline-based delta morphology classification and comparison to sediment fluxes informs our understanding of how the form and function of these densely populated and biogeochemically rich landscapes might respond to projected changes in sediment fluxes, relative sea level rise, and anthropogenic modification (Chadwick et al., 2020; Edmonds et al., 2020; Hariharan et al., 2022; Hoitink et al., 2020; Moodie & Nittrouer, 2021; Nienhuis et al., 2020; Syvitski & Saito, 2007). It also offers potential application in inferring paleoclimate from ancient delta deposits and interpreting extraterrestrial delta morphology.

Multiscale characterization of delta shorelines

We analyzed the shorelines of 54 river deltas across a range of sizes and a mixture of morphologic features (Supporting Material, Fig. 1; Syvitski & Saito, 2007). River delta shorelines were defined using the Opening Angle Method (OAM) with a critical angle of 45 degrees (Shaw et al., 2008). To define a shoreline, the OAM requires a binary water mask, which was obtained by thresholding water occurrence masks from the Landsat-derived, 30-m spatial resolution Global Surface Water dataset (Pekel et al., 2016).

We defined three scales at which delta shoreline structure exhibits variability, which are linked to the balance of river, tide, and wave forcings: a macroscale (overall delta planform), mesoscale (mouth width scale), and microscale (beach scale). We developed metrics to capture the variability at those scales as discussed below.

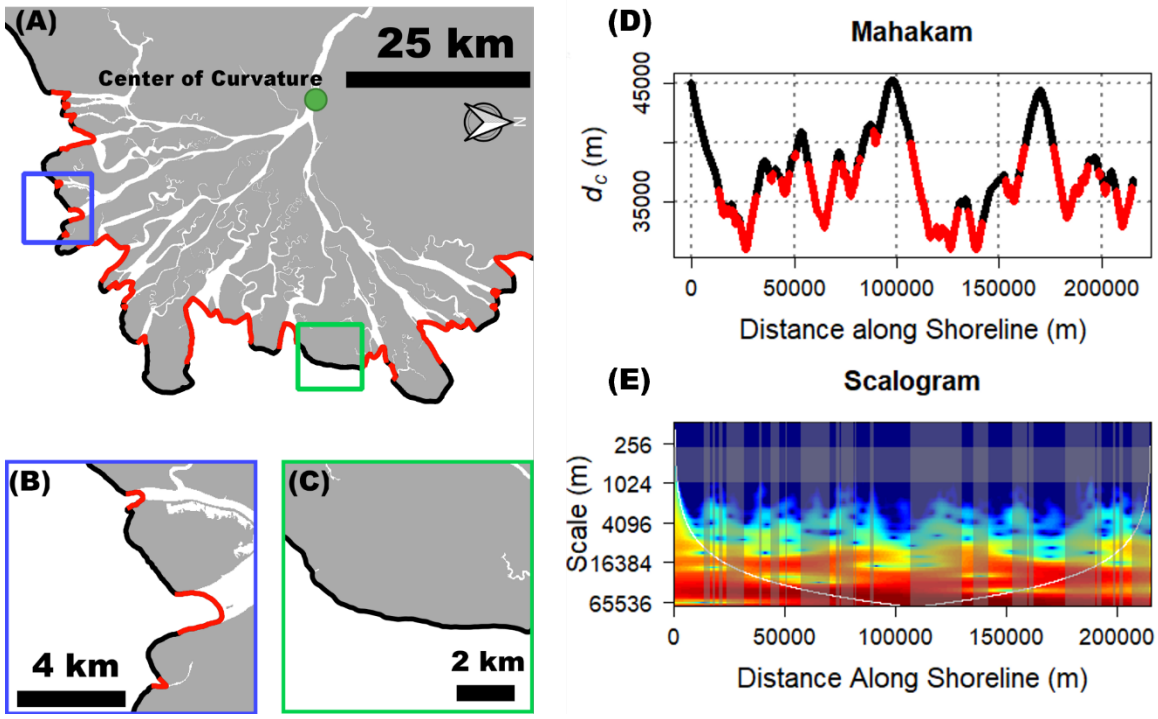

Figure 2. Example of the multiscale features of shoreline structure on the Mahakam Delta, Indonesia. (A) The shoreline of the delta, defined using the Opening Angle Method (OAM) with a critical angle of 45 degrees, shows multiple scales of variability. At the macroscale, a delta may be convex due to river deposition, flat due to wave-driven along shore transport, or concave due to tidal widening and estuarine conditions. This is measured here by the ratio between the radius of curvature and the length of the shoreline. (B) Mouths formed by rivers and tides lead to undulations in the shoreline at a scale determined by the relative river and tide fluxes. (C) At the microscale, waves diffuse sediment parallel to the coast and smooth the shoreline, while rivers and tides roughen it. (D) To measure meso- and microscale variability, the 2D shorelines are mapped to a univariate signal defined as the distance from each point along the shoreline to the center of curvature, $d_c(s)$, where s is the distance along the shoreline. (E) The wavelet transform is used to estimate the fraction of variance contributed by the mouths, fM, marked in red in the preceding panels, and the Gini-corrected Finescale Variance $gFSV$, i.e. the variance from scales (wavelengths) between 300 to 1000 m.

At the macroscale, riverine sediment deposition leads to delta progradation and growth into the receiving basin and generates extrusional shapes (i.e. convex shoreline; Caldwell & Edmonds, 2014; Galloway, 1975). When wave-driven alongshore transport removes the majority of riverine sediment flux, the delta has no protrusion, and is linear (i.e. mostly flat shoreline; Nienhuis et al., 2015). Lastly, tidal forcings erode subaerial sediment into the nearshore and construct a subaqueous platform (Hoitink et al., 2017). This net erosion from land leads to a funnel-shaped, concave subaerial delta, or estuary, which intrudes into the surrounding landscape (i.e. a concave shoreline). We therefore measured the curvature of the entire shoreline (Fig. 2; Jammalamadaka & SenGupta, 2001), to classify deltas as convex (extrusional), concave (intrusional), or flat (see Supporting Material).

At the mesoscale, the influence of rivers, waves, and tides on channel mouths dictates multiple intermediate scales of variability on the shoreline. Tidal forces widen mouths exponentially (Nienhuis et al., 2018) which leads to multiscale undulations in the shoreline (e.g. Amazon and Ganges-Brahmaputra, GBM, delta; Fig. 1). Rivers form mouth bars and bifurcations leading to small but numerous mouths, which result in intermediate to fine scale undulations in the shoreline (e.g. Dnieper delta). Lastly, wave-driven sediment transport prevents mouth bar formation (Jerolmack & Swenson, 2007) and reduces the number of channels (Broaddus et al., 2022), resulting in long shorelines with few, small undulations (e.g. Ebro delta). To measure the contribution of mouths to the overall variability of the shoreline structure, we first projected the shoreline into a univariate spatial-series by recording the distance from each point along the shoreline to the center of curvature of the macroscale shape of the delta (Fig. 2). Then, we identified sections of the shoreline spatial-series corresponding to the mouths and measured via

154 localized wavelet transforms (Kumar & Foufoula-Georgiou, 1994) the fraction of variance
155 contributed by the mouths, *fM* (Supporting Material, Fig. 2).

156 Finally, at the microscale, wave-driven alongshore transport diffuses sediment along the coast and
157 smooths shorelines (Ashton et al., 2001), while rivers and tides introduce variability from
158 distributary and headless channels (Wolinsky et al., 2010). Therefore, we measured the fine scale
159 variance (*FSV*), as the variance at wavelengths of 300 to 1000 m, to capture these differences (Fig.
160 2). The lower bound is the result of the minimum reliable scale above which discretization,
161 aliasing, and smoothing effects do not affect the spectra, derived from 30-m spatial resolution
162 Landsat imagery. The upper bound is an approximation of the range of scales within which waves
163 act to smooth shorelines and below which large scale features such as spits begin to emerge. The
164 results are robust to shifting the upper bound from 800 to 1100 m (Supporting Material).
165 Furthermore, to separate shorelines that may have equal fine scale variance but relatively more
166 power at larger wavelengths compared with shorelines that have relatively less power at those
167 wavelengths, the *FSV* is adjusted by the degree of heterogeneity over the spectral range by
168 multiplying by a spectral Gini coefficient, *g*, defining the *gFSV*. The spectral Gini coefficient is a
169 measure of the deviation of the spectra from white noise, i.e. a random signal with a flat spectrum
170 (Supporting Material). With these three metrics we quantitatively compare the shoreline
171 morphology of river deltas and explore the possible emergence of distinct morphotypes.

172 **Shoreline morphometric space**

173 The proposed shoreline metrics construct a three-dimensional Shoreline Morphometric Space
174 (SMS) within which deltas can be positioned and compared (Fig. 3). To objectively and robustly
175 identify clusters that categorically classify deltas within this space, we used an unsupervised
176 machine learning algorithm, k-prototypes (a modification of k-means clustering that accounts for

177 categorical predictors such as the macroscale shape; Huang, 1998). Five morphotypes, i.e., clusters
178 of morphologically similar deltas, emerge from the three-dimensional SMS (Fig. 3) and are
179 displayed in Fig. 4.

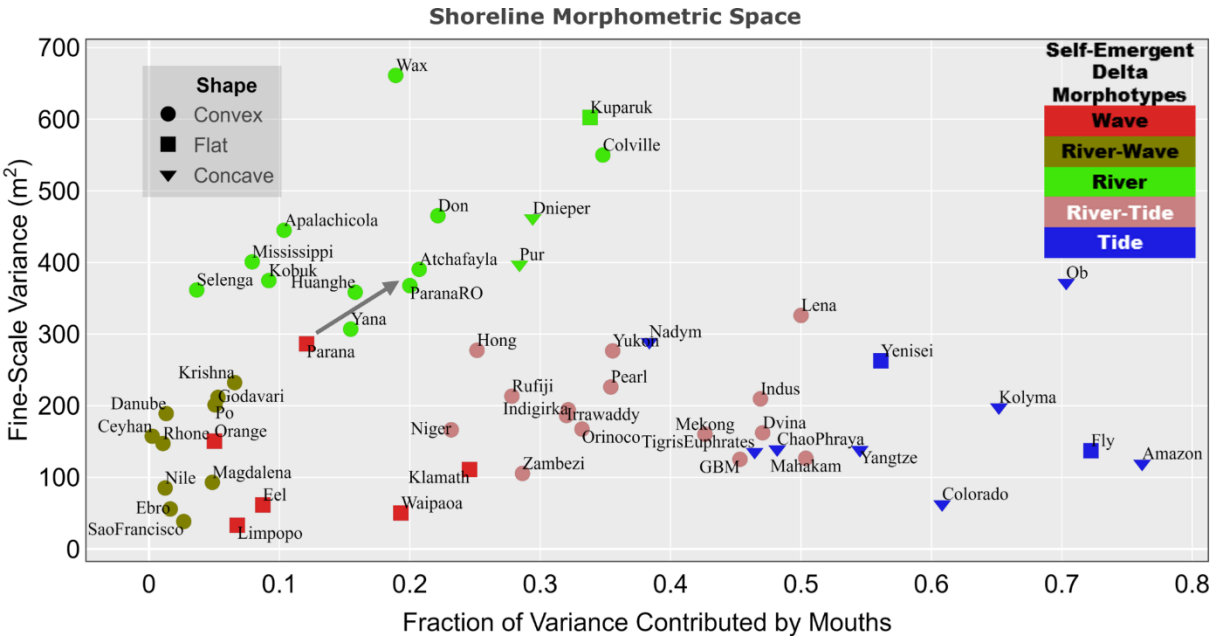

180

181 **Figure 3. The Shoreline Morphometric Space (SMS).** Deltas shorelines are positioned in the
182 three-dimensional space constructed by the macroscale shape, fM, and $gFSV$ metrics.
183 Unsupervised clustering of the SMS using k-protoypes reveals five self-emergent delta
184 morphotypes, i.e. classes of morphologically similar systems. The relative position of the deltas in
185 the SMS elucidates the dominant forcing acting on each morphotype, e.g increased *fM* a signature
186 of greater tidal influence. The classified deltas are shown in Fig. 4. The arrow indicates the shift
187 in the SMS position of the river distributary section of the Parana shoreline (ParanaRO) compared
188 with the shoreline of the entire Parana, see text for details.

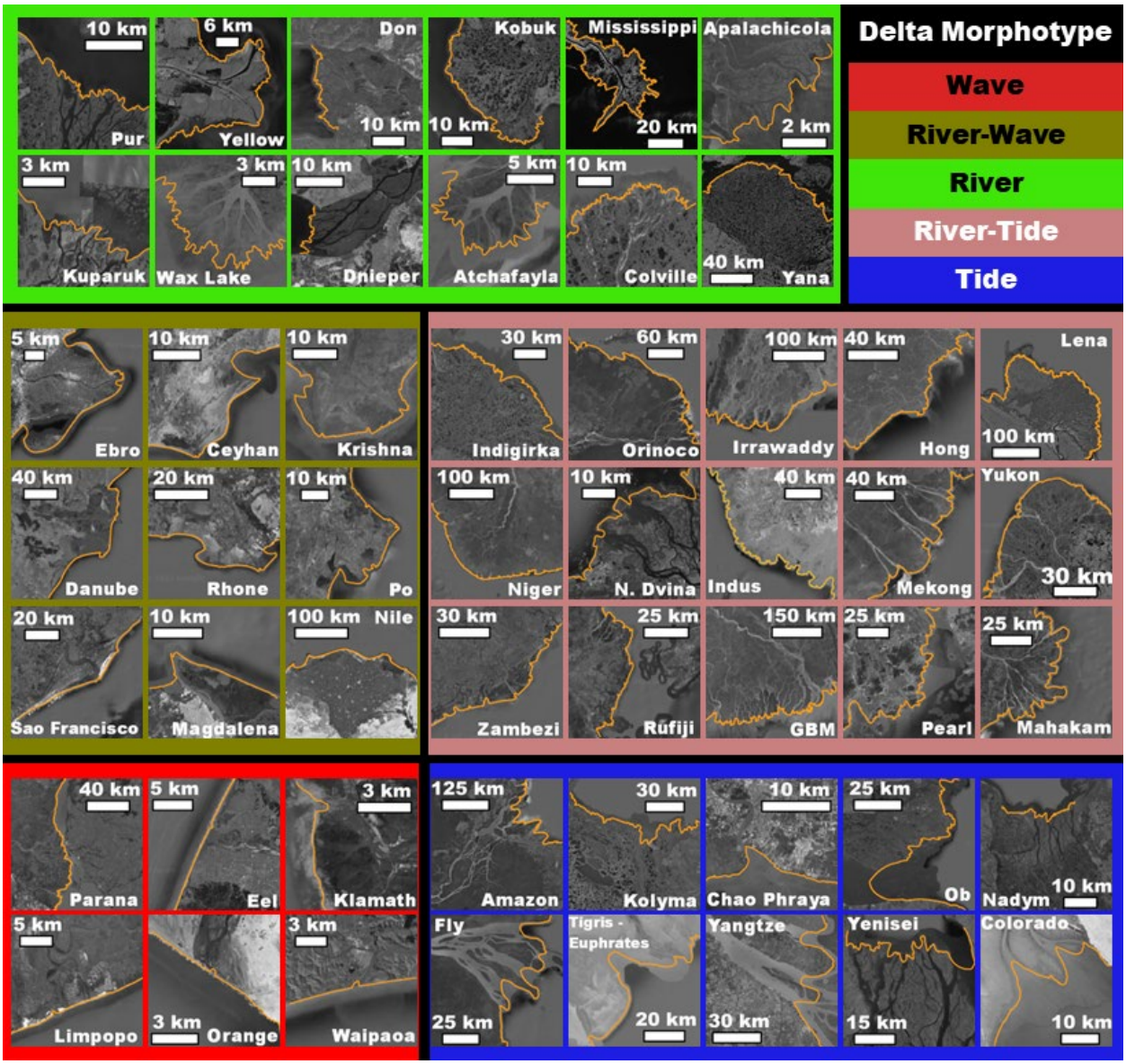

Figure 4. Deltaic morphotypes identified from the SMS. The deltas corresponding to the five morphotypes which emerged from the SMS (Fig. 3). Shorelines are shown in orange with underlying imagery from Landsat or Google Earth.

The first morphotype is denoted as the "tidal morphotype" as these deltas are concave and flat with mouth-dominated shorelines and low finescale variance, indicative of tide-domination (Fig. 4), for example, the Fly and Amazon deltas. It also includes valley-confined deltas like the Ob and

Yenisei due to their wide mouths (Fig. 4). The second morphotype is denoted as the "river morphotype" as these deltas are characterized by an intermediate fraction of variance contributed by mouths, are rough at fine scales, and have a convex planform, for example, the Selenga and Mississippi deltas (Fig. 4). Valley-confined deltas such as the Dnieper and Don, which are concave and flat but have high fine scale variability, are also included as part of the river morphotype. The third morphotype is denoted as the "wave morphotype" as these deltas are flat, lack a subaerial protrusion formed by river deposition, and smooth at fine scales, for example, the Eel and Orange deltas (Fig. 4). The fourth morphotype is denoted as the "river-wave morphotype" as these deltas are convex, smooth at fine scales, typically have spits or flying spits, and little to no variability contributed by mouths, for example, the Ebro and Rhone deltas. Lastly, the fifth morphotype is denoted as the "river-tide morphotype" as it contains convex deltas with tidally widened mouths and headless channels, resulting in intermediate variability contributed by mouths, for example, the Mahakam and Orinoco deltas.

The dominant forcings determined by the quantitative classification of shorelines correspond with expert assessment of the dominant forcings based on qualitative comparisons of delta morphology (Ainsworth et al., 2011; Nienhuis et al., 2020) suggesting that shoreline structure carries a distinct signature of the processes that generated that delta. An interesting further step is to check whether the inferred dominant forcings align with the relative sediment fluxes driven by each forcing, for which we use the recently developed sediment flux estimation framework of Nienhuis et al., (2020).

Are delta morphotypes aligned with relative sediment fluxes?

Each of the 54 deltas was projected onto the ternary Galloway diagram according to the relative sediment flux transported by rivers, waves, and tides as estimated in Nienhuis et al., (2020) (Fig

5). Before contrasting delta morphotypes with their relative sediment fluxes we note a few important issues which we anticipate to cause discrepancies in the mapping between the morphotype and dominant sediment flux. First, the marine sediment fluxes are estimated using simplified, although nonlinear, physical models which transform tidal amplitudes and offshore wave-climate into tidal and wave sediment fluxes, respectively. Therefore, any uncertainty in the tidal amplitude and wave climate will propagate into uncertainty in the sediment flux estimate. Second, sediment fluxes are estimated using single, representative locations for wave climate, tidal amplitude, and fluvial discharge, not acknowledging possible multi-mouth or multi-lobe structure (Nienhuis et al., 2020). Moreover, the sediment fluxes are estimated using contemporary wave climate, tidal amplitude measurements, and modelled, pre-anthropogenically-influenced riverine discharge and sediment loads (Supporting Material; Nienhuis et al., 2020), and represent snapshots of the relative sediment flux, while delta morphology represents the temporally integrated effect of the forcings acting on the delta (Syvitski et al., 2022). Accordingly, any significant spatiotemporal heterogeneity or non-stationarity in the fluxes over each delta's evolution might not be reflected in the contemporary sediment flux estimates. Therefore, some misalignments between delta morphotype and dominant sediment flux are expected, hoping however, that a general agreement will emerge.

The dominant forcings inferred from the delta morphotypes generally align with the estimated relative sediment fluxes driven by each forcing (Fig. 5). For example, the river morphotype and wave morphotype deltas lie in the right corners of the Galloway diagram, and the river-wave morphotype deltas span the space in-between these two end member classes with varying degree of relative tidal influence. Note that deltas in the river morphotype typically have relative river sediment flux more than 80%, although there are notable outliers. A similar observation is made

for deltas in the wave morphotype. Morphological expression of dominance by a single forcing is therefore limited only to small corners of the Galloway space. Morphologically similar deltas which appear scattered or as misalignments between shoreline-inferred dominant forcing and dominant relative sediment flux in the Galloway diagram yield valuable insight into the relationship between observed shoreline structure and the relative sediment fluxes.

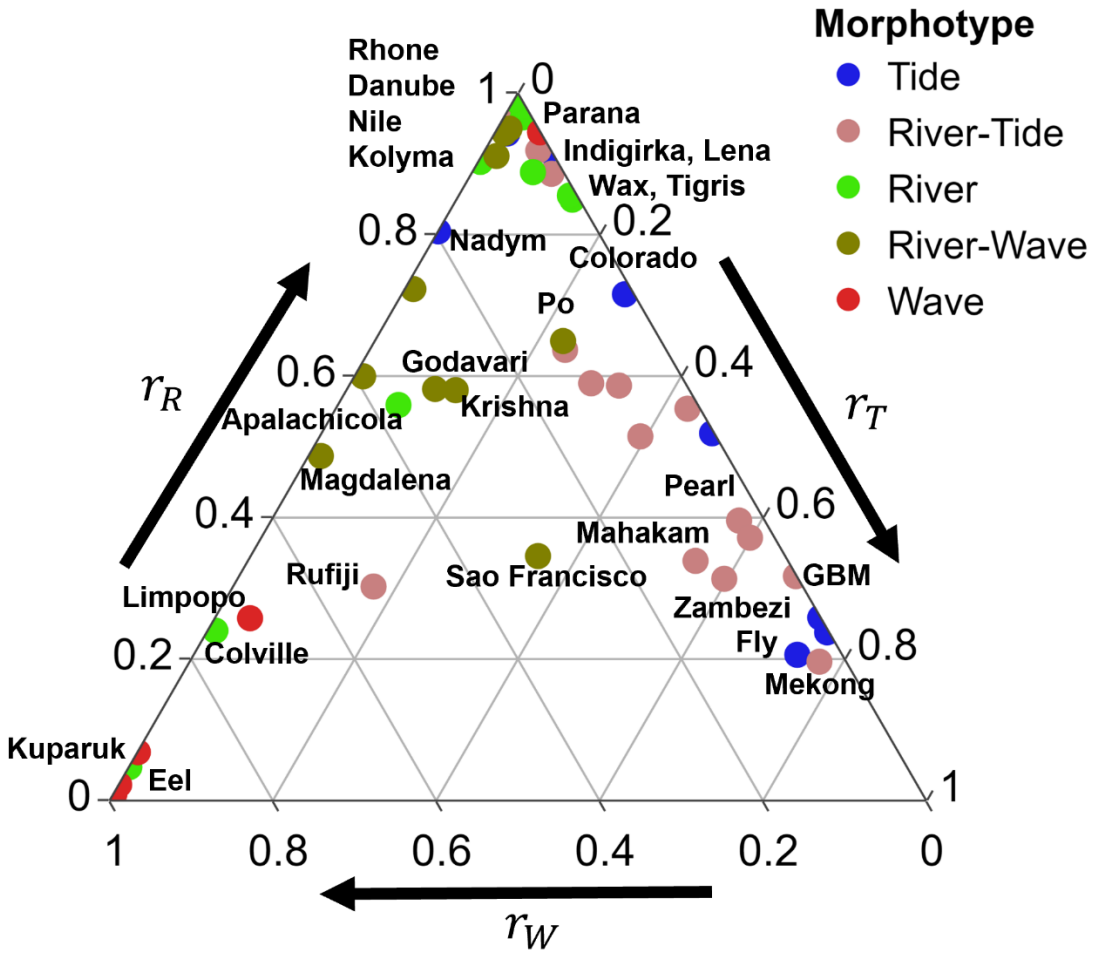

Figure 5. Comparison of delta morphotypes to sediment flux budget. The 54 deltas, colored by their morphotype emergent from the SMS (Fig. 3), are positioned in the Galloway diagram based on their estimated relative sediment fluxes (Nienhuis et al., 2020). Misalignments highlight spatiotemporal heterogeneity in the relative sediment fluxes not captured by their contemporary estimates (see text for discussion).

As discussed before, some misalignments arise due to uncertainty in the sediment fluxes estimates. For example, deltas in the tidal morphotype such as the Kolyma and Tigris-Euphrates are assigned relatively low tidal sediment fluxes (Nienhuis et al., 2020), despite displaying clear tidal widening, suggesting under-estimation of the tidal sediment fluxes for these deltas. Similarly, river morphotype deltas such as the Colville, Kuparuk, and Apalachicola, are characterized by abundant mouthbars but have high estimated wave sediment fluxes which are expected to inhibit mouthbar formation (Jerolmack & Swenson, 2007). The Kuparuk and Apalachicola are associated with valley-confined or sheltered shorelines where wave climate data may be particularly uncertain. These misalignments highlight that the shoreline morphometric approach may be more robust than the sediment flux approach for delta classification as it is less sensitive to its defining parameters (e.g. critical angle or range considered for fine scales; see Supporting Material).

Further misalignments of interest are the river-tide morphotype deltas and tide morphotype deltas which are scattered across a range of relative tidal influence. This mixture arises as the river-tide and tide morphotypes consist of deltas with intermediate to high fraction of variance contributed by mouths (*fM*) due to headless and wide channels. However, the river-tide morphotype consists solely of deltas that are convex at the macroscale, e.g. the Irrawaddy, Indus, and Mahakam, which is a signature of historical progradation of the delta planform due to fluvial deposition. Also deltas such as the Zambezi and Rufiji are convex with wide headless channels and have abundant tidal mangroves (Anthony et al., 2021; Erftemeijer & Hamerlynck, 2005), suggesting historical significant river and tidal influence, but have otherwise smooth, sandy shorelines and translating spits indicating recent wave influence. This suggests that although these systems at present have large relative tidal sediment fluxes, the estimated relative sediment fluxes do not capture the

historical river dominance which constructed them. Thus, as tides widen and preserve former distributary channels (Hoitink et al., 2017), and the timescale for waves to erase the convex depositional system formed by river progradation could be on the order of centuries (Nienhuis et al., 2016), the signature of a river remains on its delta long after it has stopped flowing. Therefore, careful consideration must be given to possible temporal heterogeneities in each of the sediment fluxes when computing their relative values and assessing the relationship between morphotype and relative sediment flux (Bhattacharya & Giosan, 2003). This is especially critical for characterizing morphologic response to sediment flux changes, e.g., decreasing riverine sediment delivery or changes in wave climate, and for projecting delta futures under climate change.

Lastly, we hypothesize that some of the misalignments arise because the morphologic metrics are computed along the length of the entire shoreline, although the sediment fluxes are computed via point estimates and don't convey information on spatial heterogeneity in the forcings acting on the delta. For example, the Parana delta lies in the wave morphotype although it has a complex distributary network in its southern half and is dominated by riverine sediment flux (Figs. 3-5). However, the Parana's depositional environment is unique as the Uruguay river runs parallel to its northern shore (Milana & Kröhling, 2015), which we posit acts as a longshore current that smoothens the shoreface but is not captured by the global sediment flux estimation framework which only includes wind-driven longshore transport. To test this hypothesis, we computed the three multiscale metrics of shoreline structure only on the section of the shoreline between the active distributaries in the southern section, terming it ParanaRO, and found that the ParanaRO indeed lies in the river morphotype (Fig. 3), in agreement with its dominant riverine sediment flux (Fig. 5).

Note that the multiscale framework presented herein allows us to further interrogate spatially explicit variability in shoreline structure. In particular, some deltas might exhibit lobes corresponding to distinct morphotypes (e.g. abandoned distributary lobes reworked by marine forces following channel avulsion), shedding further light on the alignment between sediment flux and morphology. However, the framework for estimating sediment fluxes (Nienhuis et al., 2020) will likely need to be adjusted to account for highly spatially variable sediment fluxes given multi-lobe or multi-mouth structures or variable wave climate (Syvitski et al., 2022). We note that combining shoreline metrics with metrics of network complexity (Konkol et al., 2022; Tejedor et al., 2015a, 2015b, 2016, 2017) may help to separate deltas further within the SMS and identify subnetworks that need to be treated separately in terms of their morphology and sediment fluxes. Network information may disaggregate the relatively large river-tide morphotypes and the tide morphotypes, with a possible separation of the valley-confined Ob and Yenisei deltas from estuarine systems such as the Kolyma, Ganges Brahmaputra, and Colorado. This further sub-division of deltas may also be able to yield insight into the influence of other controls on delta morphology including grain size (Caldwell & Edmonds, 2014), valley confinement, cold region processes, or sea level history (Nienhuis et al., 2023; Overeem et al., 2022). Interestingly, no systematic signature of near-shore sea-ice, permafrost, or river-ice was detected on shoreline structure (Lauzon et al., 2019; Overeem et al., 2022; Piliouras et al., 2021), except for a lack of wave influenced Arctic systems which may relate to the short wind fetch present due to sea ice (Barnhart et al., 2014) or the presence of a shallow subaqueous ramp dampening wave runup and breakup at the subaerial shoreline (Overeem et al., 2022).

Conclusion

We have introduced a novel quantitative framework to classify river delta morphology based on a multiscale characterization of delta shoreline structure through geometric and spectral metrics which form a three-dimensional shoreline morphometric space (SMS). Unsupervised classification of 54 deltas projected in the SMS reveals self-emergent morphologically similar deltas, i.e. delta morphotypes which are further associated with dominant forcings based on the metrics. We then found that dominant forcings inferred from shoreline structure generally align with the dominant forcings quantitatively estimated by their relative sediment fluxes. We posit that misalignments arise due to possible spatiotemporal variability in the dominant forcings not captured in the relative sediment fluxes, providing a basis for more detailed analysis of those deltas. The proposed shoreline morphologic classification framework relies on readily available satellite imagery making it easily applicable for remote, poorly instrumented coastlines and basins as well as on extraterrestrial bodies, for which forcings are not available.

Acknowledgements

L.V. was supported by funding from the University of California Lab Fees In Residence Graduate Fellowship Grant L21GF3569, and NASA Earth and Space Science Fellowship Grant 80NSSC18K1409. LV., A.T., H.M., C.B., and E. F-G., were supported by the United Kingdom Research \& Innovation Living Deltas Hub NES0089261. L.V., A.T., H.M., C.B., and E.F-G. were supported by the National Science Foundation through the Collaborative Research program Grant EAR1811909 while D.E., C.B., and J.B. were supported through Collaborative Research program Grant EAR1812019. J.C.R. was supported by the InteRFACE project through the DOE. J.H.N. was supported by the Dutch Research Council through Grant NWO-vi.veni.192.123. We also

344 acknowledge helpful discussion on spectral analyses with Phong V. V. Le and Clement Guilloteau,
345 as well as fruitful discussions with the CSDMS community at large.

346 **Open Research**

347 The values of each metric and relative sediment flux are available in the supplementary material
348 and will be made available via Zenodo for final publication. The Global Surface Water masks used
349 to define the shorelines are available at https://developers.google.com/earth-
350 engine/datasets/catalog/JRC_GSW1_1_GlobalSurfaceWater?hl=en. ROAM, A fast R-based
351 implementation of the Opening Angle Method, is available at http://github.com/lvulis/ROAM.

References

Adams, H., Adger, W. N., & Nicholls, R. J. (2018). Ecosystem Services Linked to Livelihoods and Well-Being in the Ganges-Brahmaputra-Meghna Delta. In *Ecosystem Services for Well-Being in Deltas* (pp. 29–47). Cham: Springer International Publishing. https://doi.org/10.1007/978-3-319-71093-8_2

Ainsworth, R. B., Vakarelov, B. K., & Nanson, R. A. (2011). Dynamic spatial and temporal prediction of changes in depositional processes on clastic shorelines: Toward improved subsurface uncertainty reduction and management. *AAPG Bulletin*, *95*(2), 267–297. https://doi.org/10.1306/06301010036

Anthony, E. J. (2015). Wave influence in the construction, shaping and destruction of river deltas: A review. *Marine Geology*, *361*, 53–78. https://doi.org/10.1016/j.margeo.2014.12.004

Anthony, E. J., Besset, M., Zainescu, F., & Goichot, M. (2021). Geomorphology of a tropical river delta under pressure: the Rufiji delta, Tanzania—context, channel connectivity and alongshore morpho-sedimentary and hydrodynamic variability. *Geo-Marine Letters*, *41*(2). https://doi.org/10.1007/s00367-021-00695-7

Ashton, A., & Giosan, L. (2011). Wave-angle control of delta evolution. *Geophysical Research Letters*, *38*(13), 1–6. https://doi.org/10.1029/2011GL047630

Ashton, A., Murray, A. B., & Arnoult, O. (2001). Formation of coastline features by large-scale instabilities induced by high-angle waves. *Nature*, *414*(6861), 296–300. https://doi.org/10.1038/35104541

Barnhart, K. R., Overeem, I., & Anderson, R. S. (2014). The effect of changing sea ice on the physical vulnerability of Arctic coasts. *Cryosphere*, *8*(5), 1777–1799. https://doi.org/10.5194/tc-8-1777-2014

Baumgardner, S. E. (2016). *Quantifying Galloway: Fluvial, Tidal and Wave Influence on Experimental and Field Deltas*.

Bhattacharya, J. P., & Giosan, L. (2003). Wave-influenced deltas: geomorphological implications for facies reconstruction. *Sedimentology*, *50*(1), 187–210. https://doi.org/10.1046/j.1365-3091.2003.00545.x

Broaddus, C. M., Vulis, L. M., Nienhuis, J. H., Tejedor, A., Brown, J., Foufoula-Georgiou, E., & Edmonds, D. A. (2022). First-Order River Delta Morphology Is Explained by the Sediment Flux Balance From Rivers, Waves, and Tides. *Geophysical Research Letters*, *49*(22). https://doi.org/10.1029/2022GL100355

Caldwell, R. L., & Edmonds, D. A. (2014). The effects of sediment properties on deltaic processes and morphologies: A numerical modeling study. *Journal of Geophysical Research: Earth Surface*, *119*(5), 961–982. https://doi.org/10.1002/2013JF002965

Chadwick, A. J., Lamb, M. P., & Ganti, V. (2020). Accelerated river avulsion frequency on lowland deltas due to sea-level rise. *Proceedings of the National Academy of Sciences of the United States of America*, *117*(30), 17584–17590. https://doi.org/10.1073/pnas.1912351117

Edmonds, D. A., Caldwell, R. L., Brondizio, E. S., & Siani, S. M. O. (2020). Coastal flooding will disproportionately impact people on river deltas. *Nature Communications*, *11*(1), 1–8. https://doi.org/10.1038/s41467-020-18531-4

Erftemeijer, P. L. A., & Hamerlynck, O. (2005). Die-Back of the Mangrove Heritiera littoralis Dryand, in the Rufiji Delta (Tanzania) Following El Niño Floods. *Journal of Coastal Research*, (42), 228–235. Retrieved from https://www.jstor.org/stable/25736988

Fagherazzi, S., Edmonds, D. A., Nardin, W., Leonardi, N., Canestrelli, A., Falcini, F., et al. (2015). Dynamics of river mouth deposits. *Reviews of Geophysics*, *53*(3), 642–672. https://doi.org/10.1002/2014RG000451

Galloway, W. E. (1975). Process framework for describing the morphological and stratigraphic evolution of deltaic depositional systems. *Deltas: Models for Exploration*, (September), 87–98.

Geleynse, N., Voller, V. R., Paola, C., & Ganti, V. (2012). Characterization of river delta shorelines. *Geophysical Research Letters*, *39*(17), 2–7. https://doi.org/10.1029/2012GL052845

Hariharan, J., Passalacqua, P., Xu, Z., Michael, H. A., Steel, E., Chadwick, A., et al. (2022). Modeling the Dynamic Response of River Deltas to Sea-Level Rise Acceleration. *Journal of Geophysical Research: Earth Surface*, *127*(9). https://doi.org/10.1029/2022JF006762

Hoitink, A. J. F., Wang, Z. B., Vermeulen, B., Huismans, Y., & Kästner, K. (2017). Tidal controls on river delta morphology. *Nature Geoscience*, *10*(9), 637–645. https://doi.org/10.1038/ngeo3000

Hoitink, A. J. F., Nittrouer, J. A., Passalacqua, P., Shaw, J. B., Langendoen, E. J., Huismans, Y., & van Maren, D. S. (2020). Resilience of River Deltas in the Anthropocene. *Journal of Geophysical Research: Earth Surface*, *125*(3), 1–24. https://doi.org/10.1029/2019JF005201

Huang, Z. (1998). Extensions to the k-Means Algorithm for Clustering Large Data Sets with Categorical Values. *Data Mining and Knowledge Discovery*, *2*(3), 283–304. https://doi.org/10.1023/A:1009769707641

Jammalamadaka, S. R., & SenGupta, A. (2001). *Topics in Circular Statistics* (Vol. 5). World Scientific. https://doi.org/10.1142/4031

Jerolmack, D. J., & Swenson, J. B. (2007). Scaling relationships and evolution of distributary networks on wave-influenced deltas. *Geophysical Research Letters*, *34*(23), 1–5. https://doi.org/10.1029/2007GL031823

Knights, D., Sawyer, A. H., Barnes, R. T., Piliouras, A., Schwenk, J., Edmonds, D. A., & Brown, A. M. (2020). Nitrate Removal Across Ecogeomorphic Zones in Wax Lake Delta, Louisiana (USA). *Water Resources Research*, *56*(8), 1–15. https://doi.org/10.1029/2019WR026867

Konkol, A., Schwenk, J., Katifori, E., & Shaw, J. B. (2022). Interplay of River and Tidal Forcings Promotes Loops in Coastal Channel Networks. *Geophysical Research Letters*, *49*(10). https://doi.org/10.1029/2022GL098284

Kumar, P., & Foufoula-Georgiou, E. (1994). *Wavelet Analysis in Geophysics: An Introduction*. *Wavelet Analysis and Its Applications* (Vol. 4). https://doi.org/10.1016/B978-0-08-052087-2.50007-4

Lauzon, R., Piliouras, A., & Rowland, J. C. (2019). Ice and permafrost effects on delta morphology and channel dynamics. *Geophysical Research Letters*, (May), 2019GL082792. https://doi.org/10.1029/2019GL082792

Milana, J. P., & Kröhling, D. (2015). Climate changes and solar cycles recorded at the Holocene Paraná Delta, and their impact on human population. *Scientific Reports*, *5*(August). https://doi.org/10.1038/srep12851

Moodie, A. J., & Nittrouer, J. A. (2021). Optimized river diversion scenarios promote sustainability of urbanized deltas. *Proceedings of the National Academy of Sciences*, *118*(27). https://doi.org/10.1073/pnas.2101649118

Nienhuis, J. H., Ashton, A. D., & Giosan, L. (2015). What makes a delta wave-dominated? *Geology*, *43*(6), 511–514. https://doi.org/10.1130/G36518.1

Nienhuis, J. H., Ashton, A. D., & Giosan, L. (2016). Littoral steering of deltaic channels. *Earth and Planetary Science Letters*, *453*(April 2018), 204–214. https://doi.org/10.1016/j.epsl.2016.08.018

Nienhuis, J. H., Hoitink, A. J. F. T., & Törnqvist, T. E. (2018). Future Change to Tide-Influenced Deltas. *Geophysical Research Letters*, *45*(8), 3499–3507. https://doi.org/10.1029/2018GL077638

Nienhuis, J. H., Ashton, A. D., Edmonds, D. A., Hoitink, A. J. F., Kettner, A. J., Rowland, J. C., & Törnqvist, T. E. (2020). Global-scale human impact on delta morphology has led to net land area gain. *Nature*, *577*(7791), 514–518. https://doi.org/10.1038/s41586-019-1905-9

Nienhuis, J. H., Kim, W., Milne, G. A., Quock, M., Slangen, A. B. A., & Törnqvist, T. E. (2023). River Deltas and Sea-Level Rise. *Annual Review of Earth and Planetary Sciences*, *51*(1). https://doi.org/10.1146/annurev-earth-031621-093732

Overeem, I., Nienhuis, J. H., & Piliouras, A. (2022). Ice-dominated Arctic deltas. *Nature Reviews Earth and Environment*, *3*(4), 225–240. https://doi.org/10.1038/s43017-022-00268-x

Pekel, J.-F., Cottam, A., Gorelick, N., & Belward, A. S. (2016). High-resolution mapping of global surface water and its long-term changes. *Nature*, *540*(7633), 418–422. https://doi.org/10.1038/nature20584

Piliouras, A., Lauzon, R., & Rowland, J. C. (2021). Unraveling the Combined Effects of Ice and Permafrost on Arctic Delta Morphodynamics. *Journal of Geophysical Research: Earth Surface*, *126*(4), 1–17. https://doi.org/10.1029/2020JF005706

Sawyer, A. H., Edmonds, D. A., & Knights, D. (2015). Surface water-groundwater connectivity in deltaic distributary channel networks. *Geophysical Research Letters*, *42*(23), 10299–10306. https://doi.org/10.1002/2015GL066156

Seybold, H., Andrade, J. S., & Herrmann, H. J. (2007). Modeling river delta formation. *Proceedings of the National Academy of Sciences of the United States of America*, *104*(43), 16804–16809. https://doi.org/10.1073/pnas.0705265104

Shaw, J. B., Wolinsky, M. A., Paola, C., & Voller, V. R. (2008). An image-based method for shoreline mapping on complex coasts. *Geophysical Research Letters*, *35*(12), 1–5. https://doi.org/10.1029/2008GL033963

Straub, K. M., Li, Q., & Benson, W. M. (2015). Influence of sediment cohesion on deltaic shoreline dynamics and bulk sediment retention: A laboratory study. *Geophysical Research Letters*, *42*(22), 9808–9815. https://doi.org/10.1002/2015GL066131

Syvitski, J., & Saito, Y. (2007). Morphodynamics of deltas under the influence of humans. *Global and Planetary Change*, *57*(3–4), 261–282. https://doi.org/10.1016/j.gloplacha.2006.12.001

Syvitski, J., Anthony, E., Saito, Y., Zăinescu, F., Day, J., Bhattacharya, J. P., & Giosan, L. (2022). Large deltas, small deltas: Toward a more rigorous understanding of coastal marine deltas. *Global and Planetary Change*, *218*. https://doi.org/10.1016/j.gloplacha.2022.103958

Tejedor, A., Longjas, A., Zaliapin, I., & Foufoula-Georgiou, E. (2015a). Delta channel networks: 1. A graph-theoretic approach for studying connectivity and steady state transport on deltaic surfaces. *Water Resources Research*, *51*(6), 3998–4018. https://doi.org/10.1002/2014WR016577

Tejedor, A., Longjas, A., Zaliapin, I., & Foufoula-Georgiou, E. (2015b). Delta channel networks: 2. Metrics of topologic and dynamic complexity for delta comparison, physical inference, and vulnerability assessment. *Water Resources Research*, *51*(6), 4019–4045. https://doi.org/10.1002/2014WR016604

Tejedor, A., Longjas, A., Caldwell, R., Edmonds, D. A., Zaliapin, I., & Foufoula-Georgiou, E. (2016). Quantifying the signature of sediment composition on the topologic and dynamic complexity of river delta channel networks and inferences toward delta classification. *Geophysical Research Letters*, *43*(7), 3280–3287. https://doi.org/10.1002/2016GL068210

494 Tejedor, A., Longjas, A., Edmonds, D. A., Zaliapin, I., Georgiou, T. T., Rinaldo, A., &
495 Foufoula-Georgiou, E. (2017). Entropy and optimality in river deltas. *Proceedings of the*
496 *National Academy of Sciences*, *114*(44), 11651–11656.
497 https://doi.org/10.1073/pnas.1708404114

498 Tognin, D., D'Alpaos, A., Marani, M., & Carniello, L. (2021). Marsh resilience to sea-level rise
499 reduced by storm-surge barriers in the Venice Lagoon. *Nature Geoscience*, *14*(12), 906–
500 911. https://doi.org/10.1038/s41561-021-00853-7

501 Wolinsky, M. A., Edmonds, D. A., Martin, J., & Paola, C. (2010). Delta allometry: Growth laws
502 for river deltas. *Geophysical Research Letters*, *37*(21), 1–6.
503 https://doi.org/10.1029/2010GL044592

504 Zoccarato, C., da Lio, C., Tosi, L., & Teatini, P. (2019). A coupled biomorpho-geomechanical
505 model of tidal marsh evolution. *Water Resources Research*, 2019WR024875.
506 https://doi.org/10.1029/2019WR024875

507

River delta morphotypes emerge from multiscale characterization of shorelines

L. Vulis[1,2], A. Tejedor[3,1], H. Ma[4,1], J. H. Nienhuis[5], C. M. Broaddus[1], J. Brown[6], D. A. Edmonds[6], J. C. Rowland[2], and E. Foufoula-Georgiou[1,7]

[1]Department of Civil and Environmental Engineering, University of California Irvine,
[2]Earth and Environmental Sciences Division, Los Alamos National Laboratory
[3]Department of Science and Engineering, Sorbonne University Abu Dhabi
[4]State Key Laboratory of Hydroscience and Engineering, Tsinghua University
[5]Department of Physical Geography, Utrecht University
[6]Department of Earth and Atmospheric Sciences, Indiana University
[7]Department of Earth System Science, University of California Irvine

Keypoints

1. Three process-informed, geometric, and spectral metrics are introduced to characterize multiscale shoreline features
2. Unsupervised clustering of the shoreline metrics reveals 5 distinct delta morphotypes which correspond to distinct forcings
3. Morphotypes can be robustly estimated from readily available satellite imagery

Abstract

Delta shoreline structure has long been hypothesized to encode information on the relative influence of fluvial, wave, and tidal processes on delta formation and evolution. We introduce here a novel multiscale characterization of shorelines by defining three process-informed morphological metrics. We show that this characterization yields self-emerging classes of morphologically similar deltas, i.e., delta morphotypes, and also predicts the dominant forcing of each morphotype. Then we show that the dominant forcings inferred from shoreline structure generally align with those estimated via relative sediment fluxes, while positing that misalignments arise from spatiotemporal heterogeneity in deltaic sediment fluxes not captured in their estimates. The proposed framework for shoreline characterization advances our quantitative understanding of how shoreline features reflect delta forcings, and may aid in deciphering paleoclimate from images of ancient deposits and projecting delta morphologic response to changes in sediment fluxes.

Plain Language Summary

It has long been posited that the observed diversity in the shapes of river deltas reflects the relative strength of river, wave, and tide forcings acting on the delta. However, rigorous quantification of delta morphology and how it relates to forcing is still lacking. Here we introduce a new multiscale geometric framework which characterizes river delta morphology via measures of its shoreline structure and then use these measures to first separate deltas into morphological classes called morphotypes and second to infer the dominant forcing of each morphotype. We then show that the dominant forcings revealed by delta shoreline structure generally align with quantitative estimates of the relative amount of sediment transported by each forcing, and posit that misalignments may reflect space-time heterogeneities in the sediment transport rates not captured in their estimated values. The proposed framework enables easy and quantifiable delta classification based on readily-available remote sensing images and may yield insight into predicting deltaic geomorphic response to changing forcings.

Introduction:

River deltas are complex ecogeomorphic landscapes which are home to upwards of 300 million people due to their fertile soils and rich ecosystems (Edmonds et al., 2020). Their intricate hydromorphology controls nearshore biogeochemical function (Knights et al., 2020; Zoccarato et al., 2019), connectivity between surface and subsurface hydrogeology and reservoirs (Sawyer et al., 2015), coastal resilience (Hoitink et al., 2020; Tognin et al., 2021), and ecosystem services (Adams et al., 2018). Deltas are particularly vulnerable to climate change due to their low relief, coastal proximity, and large populations (Edmonds et al., 2020; Hoitink et al., 2020). It is therefore critical to understand how sea level rise and changing riverine sediment loads will impact these systems (Chadwick et al., 2020; Nienhuis et al., 2023) and towards this goal, developing a

quantitative framework which links the driving forces forming deltas to delta morphology and function is imperative.

Fifty years ago, Galloway introduced the paradigm that river deltas are shaped by the interplay of progradational riverine forcings and erosional marine (wave and tide) forcings, which has steered subsequent research on river delta evolution (Galloway, 1975; see also e.g. (Ainsworth et al., 2011; Anthony, 2015; Bhattacharya & Giosan, 2003; Nienhuis et al., 2020; Seybold et al., 2007; Syvitski & Saito, 2007). The relative balance of these forcings and the multiple spatio-temporal scales at which they operate result in a stunning degree of variability in shoreline structure and channel network geometry and topology (Fagherazzi et al., 2015; Hoitink et al., 2017; Jerolmack & Swenson, 2007; Konkol et al., 2022; Tejedor et al., 2016, 2017). Rivers act to prograde the delta planform at large scales and increase roughness at fine scales via the growth of mouth bars and distributary channel expansion (Fagherazzi et al., 2015; Wolinsky et al., 2010). Waves generate alongshore transport that diffuse sediment along the shoreline at fine scales but can lead to spits at coarser scales (Ashton & Giosan, 2011) and suppress mouth-bar development (Jerolmack & Swenson, 2007). Tidal forces widen distributary channels and construct headless channels which lack connections to the upstream river, roughening the shoreline at multiple scales (Hoitink et al., 2017; Nienhuis et al., 2018).

Recently, the relative magnitudes of the forcings in the Galloway framework have been quantified via a sediment flux approach (Nienhuis et al., 2020). However, shoreline shape, a crucial ingredient in the qualitative morphological classification originally posed by Galloway (See Table 2; (Galloway, 1975), has not been quantified in a way to differentiate between visually distinct deltas, nor has been shown to have a clear relationship with forcings, e.g. (Baumgardner, 2016). This is in part because analysis of shoreline structure has typically focused on a single length scale using

metrics such as shoreline variability (Straub et al., 2015) roughness or rugosity measures (Baumgardner, 2016; Caldwell & Edmonds, 2014; Geleynse et al., 2012), and shape factors (Lauzon et al., 2019; Nienhuis et al., 2015; Wolinsky et al., 2010). Such metrics do not necessarily measure shoreline structure at process length scales, nor do they capture the multiscale variability caused by the interplay of the three driving forces.

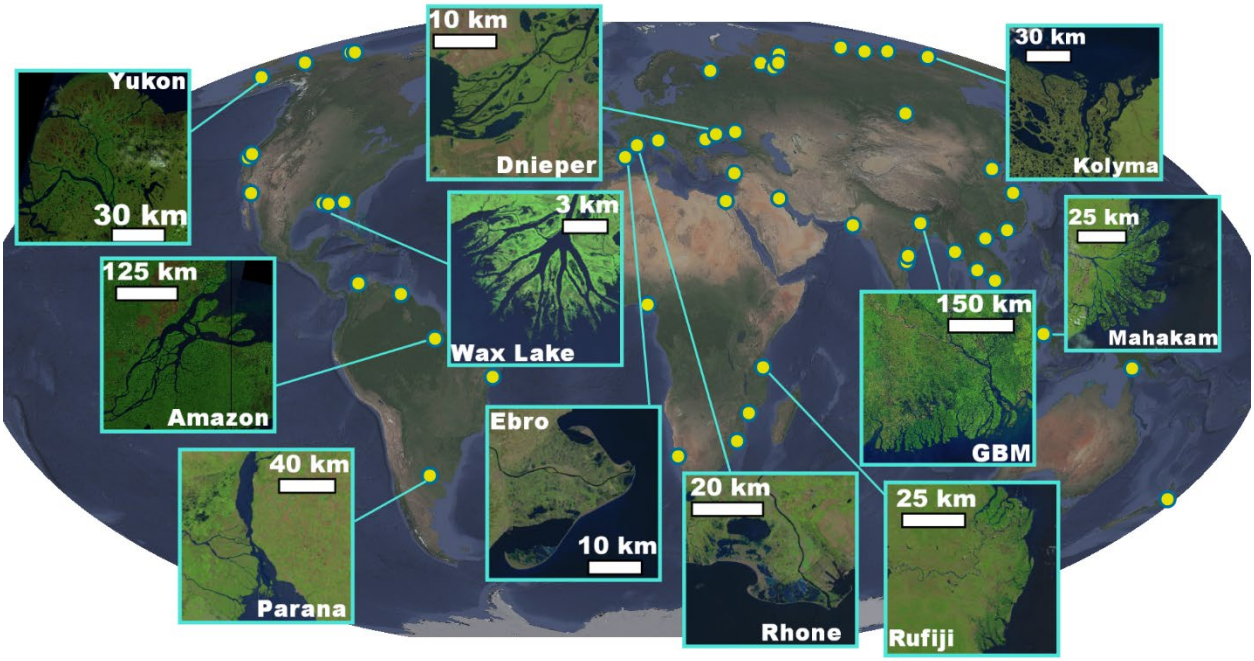

Figure 1. The morphologic variability of Earth's deltas. River deltas show differences in shoreline structure attributed to the relative balance of river, wave, and tidal sediment fluxes (Galloway, 1975). Yellow dots show locations of a globally distributed sample of 54 deltas analyzed in this study. Satellite imagery courtesy of Landsat and Google Earth.

Here, we propose a set of process-informed, multiscale metrics of river delta shoreline shape which combine geometric and spectral measures to develop a quantitative classification of delta morphology. Our approach utilizes localized analysis of shoreline structure both in space and wavenumber domains to isolate features corresponding to different processes acting at multiple scales. Unsupervised clustering of the shoreline morphometrics identifies five classes of

morphologically similar deltas, i.e. delta morphotypes. Based on the values of the process-informed metrics, dominant forcings are attributed to each morphotype, which we then show to generally align with the dominant forcings quantitatively estimated by their relative sediment fluxes (Supplementary Material; Nienhuis et al., 2020). We hypothesize that misalignments between the two are due to spatiotemporal heterogeneity in the sediment fluxes which are not captured by their estimated values. The novel shoreline-based delta morphology classification and comparison to sediment fluxes informs our understanding of how the form and function of these densely populated and biogeochemically rich landscapes might respond to projected changes in sediment fluxes, relative sea level rise, and anthropogenic modification (Chadwick et al., 2020; Edmonds et al., 2020; Hariharan et al., 2022; Hoitink et al., 2020; Moodie & Nittrouer, 2021; Nienhuis et al., 2020; Syvitski & Saito, 2007). It also offers potential application in inferring paleoclimate from ancient delta deposits and interpreting extraterrestrial delta morphology.

Multiscale characterization of delta shorelines

We analyzed the shorelines of 54 river deltas across a range of sizes and a mixture of morphologic features (Supporting Material, Fig. 1; Syvitski & Saito, 2007). River delta shorelines were defined using the Opening Angle Method (OAM) with a critical angle of 45 degrees (Shaw et al., 2008). To define a shoreline, the OAM requires a binary water mask, which was obtained by thresholding water occurrence masks from the Landsat-derived, 30-m spatial resolution Global Surface Water dataset (Pekel et al., 2016).

We defined three scales at which delta shoreline structure exhibits variability, which are linked to the balance of river, tide, and wave forcings: a macroscale (overall delta planform), mesoscale (mouth width scale), and microscale (beach scale). We developed metrics to capture the variability at those scales as discussed below.

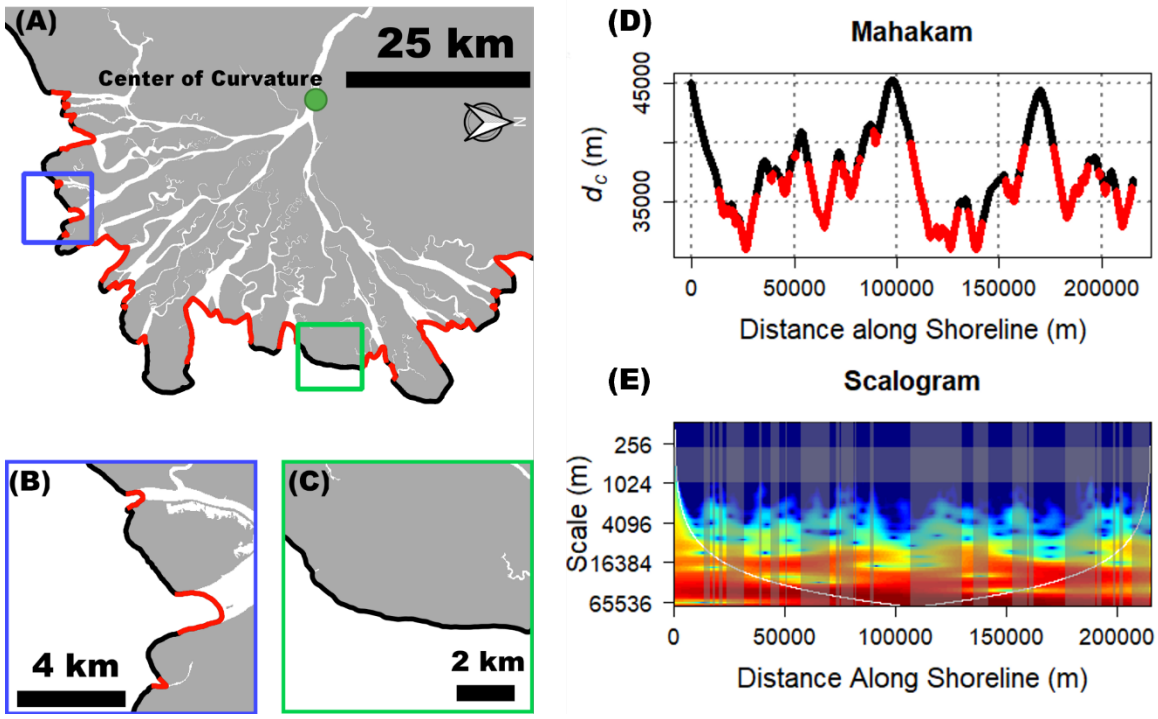

Figure 2. Example of the multiscale features of shoreline structure on the Mahakam Delta, Indonesia. (A) The shoreline of the delta, defined using the Opening Angle Method (OAM) with a critical angle of 45 degrees, shows multiple scales of variability. At the macroscale, a delta may be convex due to river deposition, flat due to wave-driven along shore transport, or concave due to tidal widening and estuarine conditions. This is measured here by the ratio between the radius of curvature and the length of the shoreline. (B) Mouths formed by rivers and tides lead to undulations in the shoreline at a scale determined by the relative river and tide fluxes. (C) At the microscale, waves diffuse sediment parallel to the coast and smooth the shoreline, while rivers and tides roughen it. (D) To measure meso- and microscale variability, the 2D shorelines are mapped to a univariate signal defined as the distance from each point along the shoreline to the center of curvature, $d_c(s)$, where s is the distance along the shoreline. (E) The wavelet transform is used to estimate the fraction of variance contributed by the mouths, fM, marked in red in the preceding panels, and the Gini-corrected Finescale Variance $gFSV$, i.e. the variance from scales (wavelengths) between 300 to 1000 m.

At the macroscale, riverine sediment deposition leads to delta progradation and growth into the receiving basin and generates extrusional shapes (i.e. convex shoreline; Caldwell & Edmonds, 2014; Galloway, 1975). When wave-driven alongshore transport removes the majority of riverine sediment flux, the delta has no protrusion, and is linear (i.e. mostly flat shoreline; Nienhuis et al., 2015). Lastly, tidal forcings erode subaerial sediment into the nearshore and construct a subaqueous platform (Hoitink et al., 2017). This net erosion from land leads to a funnel-shaped, concave subaerial delta, or estuary, which intrudes into the surrounding landscape (i.e. a concave shoreline). We therefore measured the curvature of the entire shoreline (Fig. 2; Jammalamadaka & SenGupta, 2001), to classify deltas as convex (extrusional), concave (intrusional), or flat (see Supporting Material).

At the mesoscale, the influence of rivers, waves, and tides on channel mouths dictates multiple intermediate scales of variability on the shoreline. Tidal forces widen mouths exponentially (Nienhuis et al., 2018) which leads to multiscale undulations in the shoreline (e.g. Amazon and Ganges-Brahmaputra, GBM, delta; Fig. 1). Rivers form mouth bars and bifurcations leading to small but numerous mouths, which result in intermediate to fine scale undulations in the shoreline (e.g. Dnieper delta). Lastly, wave-driven sediment transport prevents mouth bar formation (Jerolmack & Swenson, 2007) and reduces the number of channels (Broaddus et al., 2022), resulting in long shorelines with few, small undulations (e.g. Ebro delta). To measure the contribution of mouths to the overall variability of the shoreline structure, we first projected the shoreline into a univariate spatial-series by recording the distance from each point along the shoreline to the center of curvature of the macroscale shape of the delta (Fig. 2). Then, we identified sections of the shoreline spatial-series corresponding to the mouths and measured via

154 localized wavelet transforms (Kumar & Foufoula-Georgiou, 1994) the fraction of variance
155 contributed by the mouths, *fM* (Supporting Material, Fig. 2).

156 Finally, at the microscale, wave-driven alongshore transport diffuses sediment along the coast and
157 smooths shorelines (Ashton et al., 2001), while rivers and tides introduce variability from
158 distributary and headless channels (Wolinsky et al., 2010). Therefore, we measured the fine scale
159 variance (*FSV*), as the variance at wavelengths of 300 to 1000 m, to capture these differences (Fig.
160 2). The lower bound is the result of the minimum reliable scale above which discretization,
161 aliasing, and smoothing effects do not affect the spectra, derived from 30-m spatial resolution
162 Landsat imagery. The upper bound is an approximation of the range of scales within which waves
163 act to smooth shorelines and below which large scale features such as spits begin to emerge. The
164 results are robust to shifting the upper bound from 800 to 1100 m (Supporting Material).
165 Furthermore, to separate shorelines that may have equal fine scale variance but relatively more
166 power at larger wavelengths compared with shorelines that have relatively less power at those
167 wavelengths, the *FSV* is adjusted by the degree of heterogeneity over the spectral range by
168 multiplying by a spectral Gini coefficient, *g*, defining the *gFSV*. The spectral Gini coefficient is a
169 measure of the deviation of the spectra from white noise, i.e. a random signal with a flat spectrum
170 (Supporting Material). With these three metrics we quantitatively compare the shoreline
171 morphology of river deltas and explore the possible emergence of distinct morphotypes.

172 **Shoreline morphometric space**

173 The proposed shoreline metrics construct a three-dimensional Shoreline Morphometric Space
174 (SMS) within which deltas can be positioned and compared (Fig. 3). To objectively and robustly
175 identify clusters that categorically classify deltas within this space, we used an unsupervised
176 machine learning algorithm, k-prototypes (a modification of k-means clustering that accounts for

177 categorical predictors such as the macroscale shape; Huang, 1998). Five morphotypes, i.e., clusters
178 of morphologically similar deltas, emerge from the three-dimensional SMS (Fig. 3) and are
179 displayed in Fig. 4.

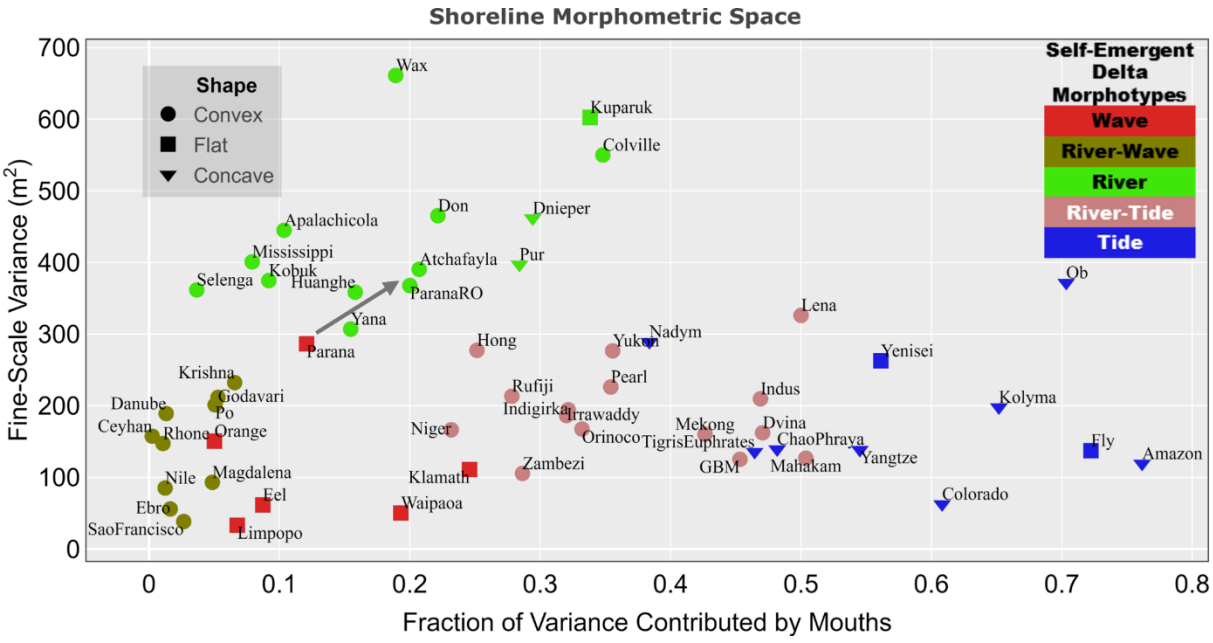

180

181 **Figure 3. The Shoreline Morphometric Space (SMS).** Deltas shorelines are positioned in the
182 three-dimensional space constructed by the macroscale shape, fM, and $gFSV$ metrics.
183 Unsupervised clustering of the SMS using k-protoypes reveals five self-emergent delta
184 morphotypes, i.e. classes of morphologically similar systems. The relative position of the deltas in
185 the SMS elucidates the dominant forcing acting on each morphotype, e.g increased *fM* a signature
186 of greater tidal influence. The classified deltas are shown in Fig. 4. The arrow indicates the shift
187 in the SMS position of the river distributary section of the Parana shoreline (ParanaRO) compared
188 with the shoreline of the entire Parana, see text for details.

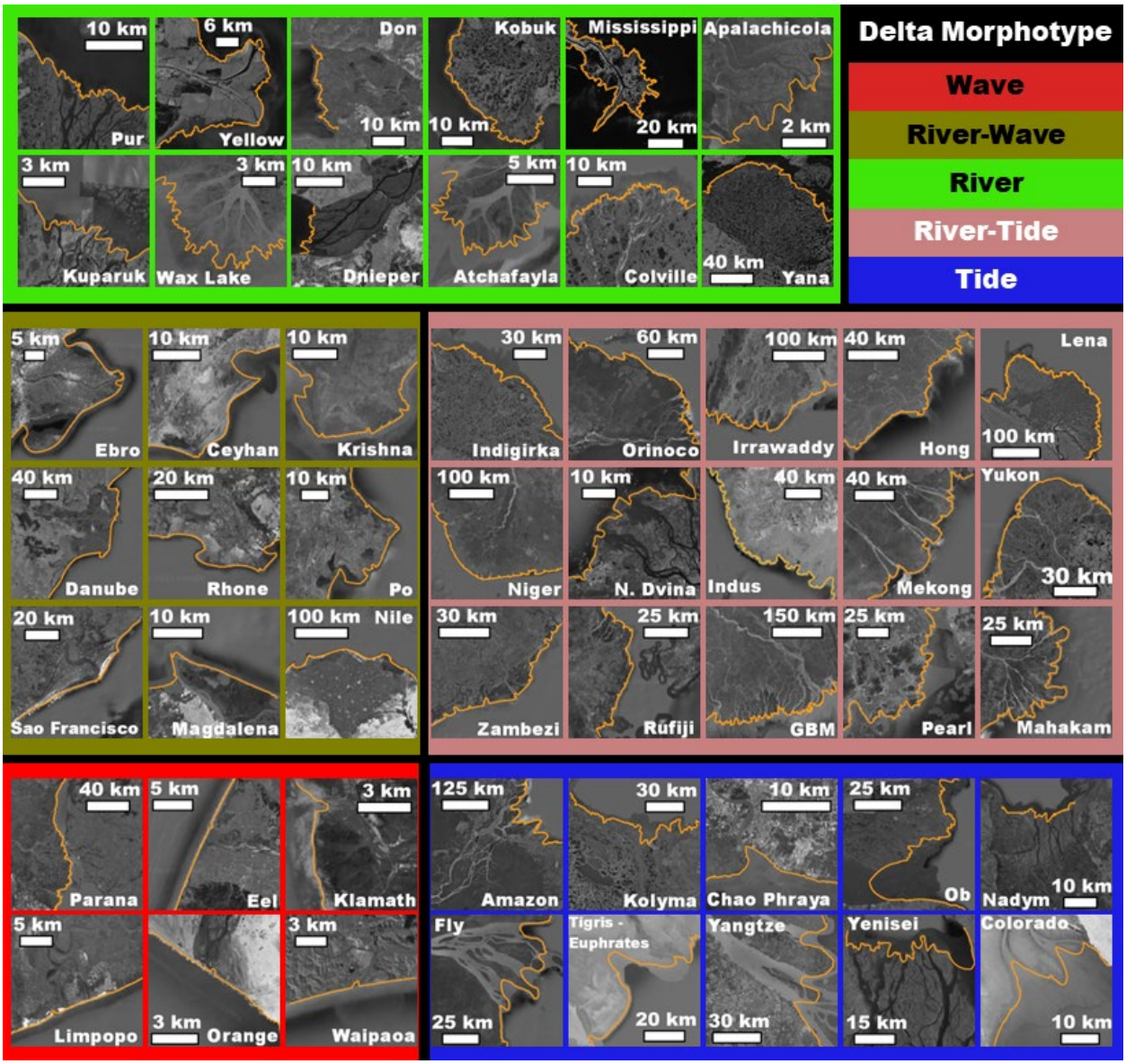

Figure 4. Deltaic morphotypes identified from the SMS. The deltas corresponding to the five morphotypes which emerged from the SMS (Fig. 3). Shorelines are shown in orange with underlying imagery from Landsat or Google Earth.

The first morphotype is denoted as the "tidal morphotype" as these deltas are concave and flat with mouth-dominated shorelines and low finescale variance, indicative of tide-domination (Fig. 4), for example, the Fly and Amazon deltas. It also includes valley-confined deltas like the Ob and

Yenisei due to their wide mouths (Fig. 4). The second morphotype is denoted as the "river morphotype" as these deltas are characterized by an intermediate fraction of variance contributed by mouths, are rough at fine scales, and have a convex planform, for example, the Selenga and Mississippi deltas (Fig. 4). Valley-confined deltas such as the Dnieper and Don, which are concave and flat but have high fine scale variability, are also included as part of the river morphotype. The third morphotype is denoted as the "wave morphotype" as these deltas are flat, lack a subaerial protrusion formed by river deposition, and smooth at fine scales, for example, the Eel and Orange deltas (Fig. 4). The fourth morphotype is denoted as the "river-wave morphotype" as these deltas are convex, smooth at fine scales, typically have spits or flying spits, and little to no variability contributed by mouths, for example, the Ebro and Rhone deltas. Lastly, the fifth morphotype is denoted as the "river-tide morphotype" as it contains convex deltas with tidally widened mouths and headless channels, resulting in intermediate variability contributed by mouths, for example, the Mahakam and Orinoco deltas.

The dominant forcings determined by the quantitative classification of shorelines correspond with expert assessment of the dominant forcings based on qualitative comparisons of delta morphology (Ainsworth et al., 2011; Nienhuis et al., 2020) suggesting that shoreline structure carries a distinct signature of the processes that generated that delta. An interesting further step is to check whether the inferred dominant forcings align with the relative sediment fluxes driven by each forcing, for which we use the recently developed sediment flux estimation framework of Nienhuis et al., (2020).

Are delta morphotypes aligned with relative sediment fluxes?

Each of the 54 deltas was projected onto the ternary Galloway diagram according to the relative sediment flux transported by rivers, waves, and tides as estimated in Nienhuis et al., (2020) (Fig

5). Before contrasting delta morphotypes with their relative sediment fluxes we note a few important issues which we anticipate to cause discrepancies in the mapping between the morphotype and dominant sediment flux. First, the marine sediment fluxes are estimated using simplified, although nonlinear, physical models which transform tidal amplitudes and offshore wave-climate into tidal and wave sediment fluxes, respectively. Therefore, any uncertainty in the tidal amplitude and wave climate will propagate into uncertainty in the sediment flux estimate. Second, sediment fluxes are estimated using single, representative locations for wave climate, tidal amplitude, and fluvial discharge, not acknowledging possible multi-mouth or multi-lobe structure (Nienhuis et al., 2020). Moreover, the sediment fluxes are estimated using contemporary wave climate, tidal amplitude measurements, and modelled, pre-anthropogenically-influenced riverine discharge and sediment loads (Supporting Material; Nienhuis et al., 2020), and represent snapshots of the relative sediment flux, while delta morphology represents the temporally integrated effect of the forcings acting on the delta (Syvitski et al., 2022). Accordingly, any significant spatiotemporal heterogeneity or non-stationarity in the fluxes over each delta's evolution might not be reflected in the contemporary sediment flux estimates. Therefore, some misalignments between delta morphotype and dominant sediment flux are expected, hoping however, that a general agreement will emerge.

The dominant forcings inferred from the delta morphotypes generally align with the estimated relative sediment fluxes driven by each forcing (Fig. 5). For example, the river morphotype and wave morphotype deltas lie in the right corners of the Galloway diagram, and the river-wave morphotype deltas span the space in-between these two end member classes with varying degree of relative tidal influence. Note that deltas in the river morphotype typically have relative river sediment flux more than 80%, although there are notable outliers. A similar observation is made

for deltas in the wave morphotype. Morphological expression of dominance by a single forcing is therefore limited only to small corners of the Galloway space. Morphologically similar deltas which appear scattered or as misalignments between shoreline-inferred dominant forcing and dominant relative sediment flux in the Galloway diagram yield valuable insight into the relationship between observed shoreline structure and the relative sediment fluxes.

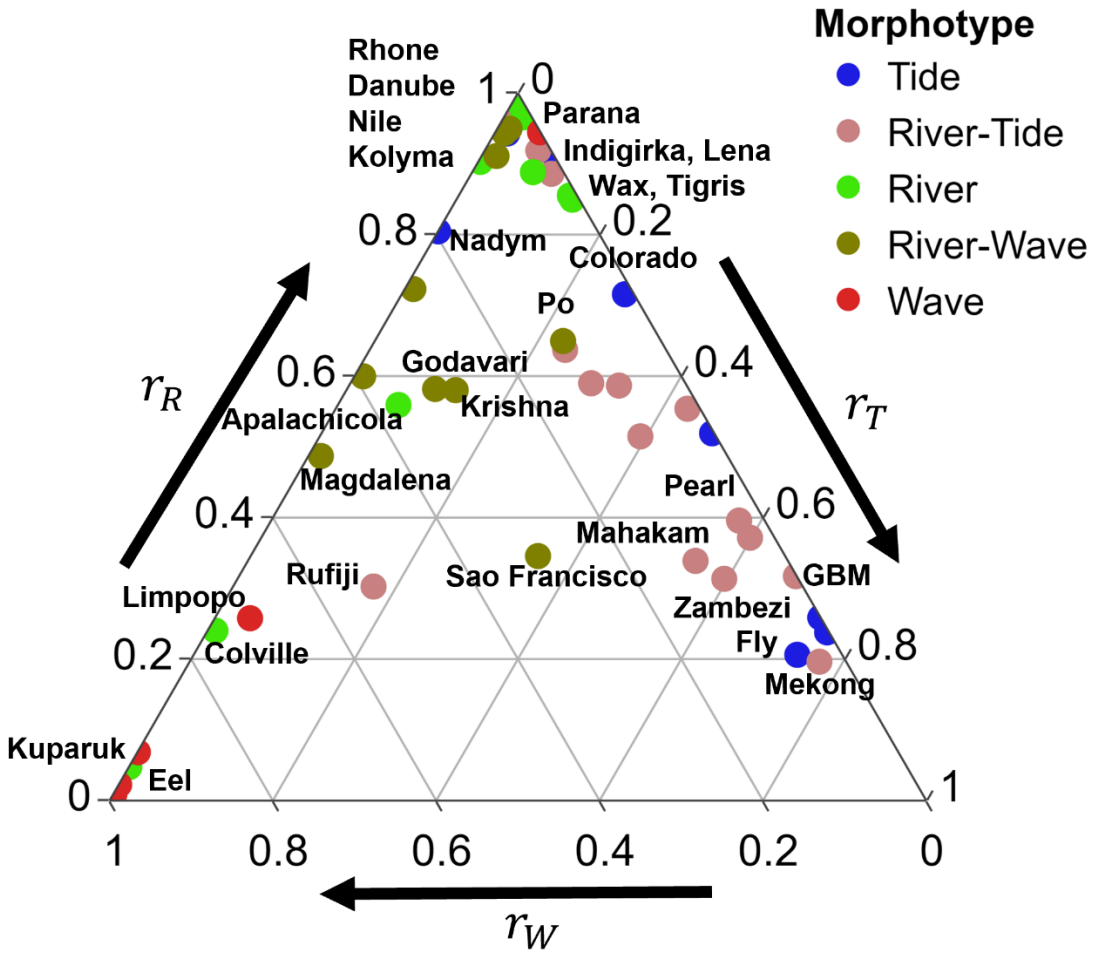

Figure 5. Comparison of delta morphotypes to sediment flux budget. The 54 deltas, colored by their morphotype emergent from the SMS (Fig. 3), are positioned in the Galloway diagram based on their estimated relative sediment fluxes (Nienhuis et al., 2020). Misalignments highlight spatiotemporal heterogeneity in the relative sediment fluxes not captured by their contemporary estimates (see text for discussion).

As discussed before, some misalignments arise due to uncertainty in the sediment fluxes estimates. For example, deltas in the tidal morphotype such as the Kolyma and Tigris-Euphrates are assigned relatively low tidal sediment fluxes (Nienhuis et al., 2020), despite displaying clear tidal widening, suggesting under-estimation of the tidal sediment fluxes for these deltas. Similarly, river morphotype deltas such as the Colville, Kuparuk, and Apalachicola, are characterized by abundant mouthbars but have high estimated wave sediment fluxes which are expected to inhibit mouthbar formation (Jerolmack & Swenson, 2007). The Kuparuk and Apalachicola are associated with valley-confined or sheltered shorelines where wave climate data may be particularly uncertain. These misalignments highlight that the shoreline morphometric approach may be more robust than the sediment flux approach for delta classification as it is less sensitive to its defining parameters (e.g. critical angle or range considered for fine scales; see Supporting Material).

Further misalignments of interest are the river-tide morphotype deltas and tide morphotype deltas which are scattered across a range of relative tidal influence. This mixture arises as the river-tide and tide morphotypes consist of deltas with intermediate to high fraction of variance contributed by mouths (*fM*) due to headless and wide channels. However, the river-tide morphotype consists solely of deltas that are convex at the macroscale, e.g. the Irrawaddy, Indus, and Mahakam, which is a signature of historical progradation of the delta planform due to fluvial deposition. Also deltas such as the Zambezi and Rufiji are convex with wide headless channels and have abundant tidal mangroves (Anthony et al., 2021; Erftemeijer & Hamerlynck, 2005), suggesting historical significant river and tidal influence, but have otherwise smooth, sandy shorelines and translating spits indicating recent wave influence. This suggests that although these systems at present have large relative tidal sediment fluxes, the estimated relative sediment fluxes do not capture the

historical river dominance which constructed them. Thus, as tides widen and preserve former distributary channels (Hoitink et al., 2017), and the timescale for waves to erase the convex depositional system formed by river progradation could be on the order of centuries (Nienhuis et al., 2016), the signature of a river remains on its delta long after it has stopped flowing. Therefore, careful consideration must be given to possible temporal heterogeneities in each of the sediment fluxes when computing their relative values and assessing the relationship between morphotype and relative sediment flux (Bhattacharya & Giosan, 2003). This is especially critical for characterizing morphologic response to sediment flux changes, e.g., decreasing riverine sediment delivery or changes in wave climate, and for projecting delta futures under climate change.

Lastly, we hypothesize that some of the misalignments arise because the morphologic metrics are computed along the length of the entire shoreline, although the sediment fluxes are computed via point estimates and don't convey information on spatial heterogeneity in the forcings acting on the delta. For example, the Parana delta lies in the wave morphotype although it has a complex distributary network in its southern half and is dominated by riverine sediment flux (Figs. 3-5). However, the Parana's depositional environment is unique as the Uruguay river runs parallel to its northern shore (Milana & Kröhling, 2015), which we posit acts as a longshore current that smoothens the shoreface but is not captured by the global sediment flux estimation framework which only includes wind-driven longshore transport. To test this hypothesis, we computed the three multiscale metrics of shoreline structure only on the section of the shoreline between the active distributaries in the southern section, terming it ParanaRO, and found that the ParanaRO indeed lies in the river morphotype (Fig. 3), in agreement with its dominant riverine sediment flux (Fig. 5).

Note that the multiscale framework presented herein allows us to further interrogate spatially explicit variability in shoreline structure. In particular, some deltas might exhibit lobes corresponding to distinct morphotypes (e.g. abandoned distributary lobes reworked by marine forces following channel avulsion), shedding further light on the alignment between sediment flux and morphology. However, the framework for estimating sediment fluxes (Nienhuis et al., 2020) will likely need to be adjusted to account for highly spatially variable sediment fluxes given multi-lobe or multi-mouth structures or variable wave climate (Syvitski et al., 2022). We note that combining shoreline metrics with metrics of network complexity (Konkol et al., 2022; Tejedor et al., 2015a, 2015b, 2016, 2017) may help to separate deltas further within the SMS and identify subnetworks that need to be treated separately in terms of their morphology and sediment fluxes. Network information may disaggregate the relatively large river-tide morphotypes and the tide morphotypes, with a possible separation of the valley-confined Ob and Yenisei deltas from estuarine systems such as the Kolyma, Ganges Brahmaputra, and Colorado. This further sub-division of deltas may also be able to yield insight into the influence of other controls on delta morphology including grain size (Caldwell & Edmonds, 2014), valley confinement, cold region processes, or sea level history (Nienhuis et al., 2023; Overeem et al., 2022). Interestingly, no systematic signature of near-shore sea-ice, permafrost, or river-ice was detected on shoreline structure (Lauzon et al., 2019; Overeem et al., 2022; Piliouras et al., 2021), except for a lack of wave influenced Arctic systems which may relate to the short wind fetch present due to sea ice (Barnhart et al., 2014) or the presence of a shallow subaqueous ramp dampening wave runup and breakup at the subaerial shoreline (Overeem et al., 2022).

Conclusion

We have introduced a novel quantitative framework to classify river delta morphology based on a multiscale characterization of delta shoreline structure through geometric and spectral metrics which form a three-dimensional shoreline morphometric space (SMS). Unsupervised classification of 54 deltas projected in the SMS reveals self-emergent morphologically similar deltas, i.e. delta morphotypes which are further associated with dominant forcings based on the metrics. We then found that dominant forcings inferred from shoreline structure generally align with the dominant forcings quantitatively estimated by their relative sediment fluxes. We posit that misalignments arise due to possible spatiotemporal variability in the dominant forcings not captured in the relative sediment fluxes, providing a basis for more detailed analysis of those deltas. The proposed shoreline morphologic classification framework relies on readily available satellite imagery making it easily applicable for remote, poorly instrumented coastlines and basins as well as on extraterrestrial bodies, for which forcings are not available.

Acknowledgements

L.V. was supported by funding from the University of California Lab Fees In Residence Graduate Fellowship Grant L21GF3569, and NASA Earth and Space Science Fellowship Grant 80NSSC18K1409. LV., A.T., H.M., C.B., and E. F-G., were supported by the United Kingdom Research \& Innovation Living Deltas Hub NES0089261. L.V., A.T., H.M., C.B., and E.F-G. were supported by the National Science Foundation through the Collaborative Research program Grant EAR1811909 while D.E., C.B., and J.B. were supported through Collaborative Research program Grant EAR1812019. J.C.R. was supported by the InteRFACE project through the DOE. J.H.N. was supported by the Dutch Research Council through Grant NWO-vi.veni.192.123. We also

344 acknowledge helpful discussion on spectral analyses with Phong V. V. Le and Clement Guilloteau,
345 as well as fruitful discussions with the CSDMS community at large.

346 **Open Research**

347 The values of each metric and relative sediment flux are available in the supplementary material
348 and will be made available via Zenodo for final publication. The Global Surface Water masks used
349 to define the shorelines are available at https://developers.google.com/earth-
350 engine/datasets/catalog/JRC_GSW1_1_GlobalSurfaceWater?hl=en. ROAM, A fast R-based
351 implementation of the Opening Angle Method, is available at http://github.com/lvulis/ROAM.

References

Adams, H., Adger, W. N., & Nicholls, R. J. (2018). Ecosystem Services Linked to Livelihoods and Well-Being in the Ganges-Brahmaputra-Meghna Delta. In *Ecosystem Services for Well-Being in Deltas* (pp. 29–47). Cham: Springer International Publishing. https://doi.org/10.1007/978-3-319-71093-8_2

Ainsworth, R. B., Vakarelov, B. K., & Nanson, R. A. (2011). Dynamic spatial and temporal prediction of changes in depositional processes on clastic shorelines: Toward improved subsurface uncertainty reduction and management. *AAPG Bulletin*, *95*(2), 267–297. https://doi.org/10.1306/06301010036

Anthony, E. J. (2015). Wave influence in the construction, shaping and destruction of river deltas: A review. *Marine Geology*, *361*, 53–78. https://doi.org/10.1016/j.margeo.2014.12.004

Anthony, E. J., Besset, M., Zainescu, F., & Goichot, M. (2021). Geomorphology of a tropical river delta under pressure: the Rufiji delta, Tanzania—context, channel connectivity and alongshore morpho-sedimentary and hydrodynamic variability. *Geo-Marine Letters*, *41*(2). https://doi.org/10.1007/s00367-021-00695-7

Ashton, A., & Giosan, L. (2011). Wave-angle control of delta evolution. *Geophysical Research Letters*, *38*(13), 1–6. https://doi.org/10.1029/2011GL047630

Ashton, A., Murray, A. B., & Arnoult, O. (2001). Formation of coastline features by large-scale instabilities induced by high-angle waves. *Nature*, *414*(6861), 296–300. https://doi.org/10.1038/35104541

Barnhart, K. R., Overeem, I., & Anderson, R. S. (2014). The effect of changing sea ice on the physical vulnerability of Arctic coasts. *Cryosphere*, *8*(5), 1777–1799. https://doi.org/10.5194/tc-8-1777-2014

Baumgardner, S. E. (2016). *Quantifying Galloway: Fluvial, Tidal and Wave Influence on Experimental and Field Deltas*.

Bhattacharya, J. P., & Giosan, L. (2003). Wave-influenced deltas: geomorphological implications for facies reconstruction. *Sedimentology*, *50*(1), 187–210. https://doi.org/10.1046/j.1365-3091.2003.00545.x

Broaddus, C. M., Vulis, L. M., Nienhuis, J. H., Tejedor, A., Brown, J., Foufoula-Georgiou, E., & Edmonds, D. A. (2022). First-Order River Delta Morphology Is Explained by the Sediment Flux Balance From Rivers, Waves, and Tides. *Geophysical Research Letters*, *49*(22). https://doi.org/10.1029/2022GL100355

Caldwell, R. L., & Edmonds, D. A. (2014). The effects of sediment properties on deltaic processes and morphologies: A numerical modeling study. *Journal of Geophysical Research: Earth Surface*, *119*(5), 961–982. https://doi.org/10.1002/2013JF002965

Chadwick, A. J., Lamb, M. P., & Ganti, V. (2020). Accelerated river avulsion frequency on lowland deltas due to sea-level rise. *Proceedings of the National Academy of Sciences of the United States of America*, *117*(30), 17584–17590. https://doi.org/10.1073/pnas.1912351117

Edmonds, D. A., Caldwell, R. L., Brondizio, E. S., & Siani, S. M. O. (2020). Coastal flooding will disproportionately impact people on river deltas. *Nature Communications*, *11*(1), 1–8. https://doi.org/10.1038/s41467-020-18531-4

Erftemeijer, P. L. A., & Hamerlynck, O. (2005). Die-Back of the Mangrove Heritiera littoralis Dryand, in the Rufiji Delta (Tanzania) Following El Niño Floods. *Journal of Coastal Research*, (42), 228–235. Retrieved from https://www.jstor.org/stable/25736988

Fagherazzi, S., Edmonds, D. A., Nardin, W., Leonardi, N., Canestrelli, A., Falcini, F., et al. (2015). Dynamics of river mouth deposits. *Reviews of Geophysics*, *53*(3), 642–672. https://doi.org/10.1002/2014RG000451

Galloway, W. E. (1975). Process framework for describing the morphological and stratigraphic evolution of deltaic depositional systems. *Deltas: Models for Exploration*, (September), 87–98.

Geleynse, N., Voller, V. R., Paola, C., & Ganti, V. (2012). Characterization of river delta shorelines. *Geophysical Research Letters*, *39*(17), 2–7. https://doi.org/10.1029/2012GL052845

Hariharan, J., Passalacqua, P., Xu, Z., Michael, H. A., Steel, E., Chadwick, A., et al. (2022). Modeling the Dynamic Response of River Deltas to Sea-Level Rise Acceleration. *Journal of Geophysical Research: Earth Surface*, *127*(9). https://doi.org/10.1029/2022JF006762

Hoitink, A. J. F., Wang, Z. B., Vermeulen, B., Huismans, Y., & Kästner, K. (2017). Tidal controls on river delta morphology. *Nature Geoscience*, *10*(9), 637–645. https://doi.org/10.1038/ngeo3000

Hoitink, A. J. F., Nittrouer, J. A., Passalacqua, P., Shaw, J. B., Langendoen, E. J., Huismans, Y., & van Maren, D. S. (2020). Resilience of River Deltas in the Anthropocene. *Journal of Geophysical Research: Earth Surface*, *125*(3), 1–24. https://doi.org/10.1029/2019JF005201

Huang, Z. (1998). Extensions to the k-Means Algorithm for Clustering Large Data Sets with Categorical Values. *Data Mining and Knowledge Discovery*, *2*(3), 283–304. https://doi.org/10.1023/A:1009769707641

Jammalamadaka, S. R., & SenGupta, A. (2001). *Topics in Circular Statistics* (Vol. 5). World Scientific. https://doi.org/10.1142/4031

Jerolmack, D. J., & Swenson, J. B. (2007). Scaling relationships and evolution of distributary networks on wave-influenced deltas. *Geophysical Research Letters*, *34*(23), 1–5. https://doi.org/10.1029/2007GL031823

Knights, D., Sawyer, A. H., Barnes, R. T., Piliouras, A., Schwenk, J., Edmonds, D. A., & Brown, A. M. (2020). Nitrate Removal Across Ecogeomorphic Zones in Wax Lake Delta, Louisiana (USA). *Water Resources Research*, *56*(8), 1–15. https://doi.org/10.1029/2019WR026867

Konkol, A., Schwenk, J., Katifori, E., & Shaw, J. B. (2022). Interplay of River and Tidal Forcings Promotes Loops in Coastal Channel Networks. *Geophysical Research Letters*, *49*(10). https://doi.org/10.1029/2022GL098284

Kumar, P., & Foufoula-Georgiou, E. (1994). *Wavelet Analysis in Geophysics: An Introduction*. *Wavelet Analysis and Its Applications* (Vol. 4). https://doi.org/10.1016/B978-0-08-052087-2.50007-4

Lauzon, R., Piliouras, A., & Rowland, J. C. (2019). Ice and permafrost effects on delta morphology and channel dynamics. *Geophysical Research Letters*, (May), 2019GL082792. https://doi.org/10.1029/2019GL082792

Milana, J. P., & Kröhling, D. (2015). Climate changes and solar cycles recorded at the Holocene Paraná Delta, and their impact on human population. *Scientific Reports*, *5*(August). https://doi.org/10.1038/srep12851

Moodie, A. J., & Nittrouer, J. A. (2021). Optimized river diversion scenarios promote sustainability of urbanized deltas. *Proceedings of the National Academy of Sciences*, *118*(27). https://doi.org/10.1073/pnas.2101649118

Nienhuis, J. H., Ashton, A. D., & Giosan, L. (2015). What makes a delta wave-dominated? *Geology*, *43*(6), 511–514. https://doi.org/10.1130/G36518.1

Nienhuis, J. H., Ashton, A. D., & Giosan, L. (2016). Littoral steering of deltaic channels. *Earth and Planetary Science Letters*, *453*(April 2018), 204–214. https://doi.org/10.1016/j.epsl.2016.08.018

Nienhuis, J. H., Hoitink, A. J. F. T., & Törnqvist, T. E. (2018). Future Change to Tide-Influenced Deltas. *Geophysical Research Letters*, *45*(8), 3499–3507. https://doi.org/10.1029/2018GL077638

Nienhuis, J. H., Ashton, A. D., Edmonds, D. A., Hoitink, A. J. F., Kettner, A. J., Rowland, J. C., & Törnqvist, T. E. (2020). Global-scale human impact on delta morphology has led to net land area gain. *Nature*, *577*(7791), 514–518. https://doi.org/10.1038/s41586-019-1905-9

Nienhuis, J. H., Kim, W., Milne, G. A., Quock, M., Slangen, A. B. A., & Törnqvist, T. E. (2023). River Deltas and Sea-Level Rise. *Annual Review of Earth and Planetary Sciences*, *51*(1). https://doi.org/10.1146/annurev-earth-031621-093732

Overeem, I., Nienhuis, J. H., & Piliouras, A. (2022). Ice-dominated Arctic deltas. *Nature Reviews Earth and Environment*, *3*(4), 225–240. https://doi.org/10.1038/s43017-022-00268-x

Pekel, J.-F., Cottam, A., Gorelick, N., & Belward, A. S. (2016). High-resolution mapping of global surface water and its long-term changes. *Nature*, *540*(7633), 418–422. https://doi.org/10.1038/nature20584

Piliouras, A., Lauzon, R., & Rowland, J. C. (2021). Unraveling the Combined Effects of Ice and Permafrost on Arctic Delta Morphodynamics. *Journal of Geophysical Research: Earth Surface*, *126*(4), 1–17. https://doi.org/10.1029/2020JF005706

Sawyer, A. H., Edmonds, D. A., & Knights, D. (2015). Surface water-groundwater connectivity in deltaic distributary channel networks. *Geophysical Research Letters*, *42*(23), 10299–10306. https://doi.org/10.1002/2015GL066156

Seybold, H., Andrade, J. S., & Herrmann, H. J. (2007). Modeling river delta formation. *Proceedings of the National Academy of Sciences of the United States of America*, *104*(43), 16804–16809. https://doi.org/10.1073/pnas.0705265104

Shaw, J. B., Wolinsky, M. A., Paola, C., & Voller, V. R. (2008). An image-based method for shoreline mapping on complex coasts. *Geophysical Research Letters*, *35*(12), 1–5. https://doi.org/10.1029/2008GL033963

Straub, K. M., Li, Q., & Benson, W. M. (2015). Influence of sediment cohesion on deltaic shoreline dynamics and bulk sediment retention: A laboratory study. *Geophysical Research Letters*, *42*(22), 9808–9815. https://doi.org/10.1002/2015GL066131

Syvitski, J., & Saito, Y. (2007). Morphodynamics of deltas under the influence of humans. *Global and Planetary Change*, *57*(3–4), 261–282. https://doi.org/10.1016/j.gloplacha.2006.12.001

Syvitski, J., Anthony, E., Saito, Y., Zăinescu, F., Day, J., Bhattacharya, J. P., & Giosan, L. (2022). Large deltas, small deltas: Toward a more rigorous understanding of coastal marine deltas. *Global and Planetary Change*, *218*. https://doi.org/10.1016/j.gloplacha.2022.103958

Tejedor, A., Longjas, A., Zaliapin, I., & Foufoula-Georgiou, E. (2015a). Delta channel networks: 1. A graph-theoretic approach for studying connectivity and steady state transport on deltaic surfaces. *Water Resources Research*, *51*(6), 3998–4018. https://doi.org/10.1002/2014WR016577

Tejedor, A., Longjas, A., Zaliapin, I., & Foufoula-Georgiou, E. (2015b). Delta channel networks: 2. Metrics of topologic and dynamic complexity for delta comparison, physical inference, and vulnerability assessment. *Water Resources Research*, *51*(6), 4019–4045. https://doi.org/10.1002/2014WR016604

Tejedor, A., Longjas, A., Caldwell, R., Edmonds, D. A., Zaliapin, I., & Foufoula-Georgiou, E. (2016). Quantifying the signature of sediment composition on the topologic and dynamic complexity of river delta channel networks and inferences toward delta classification. *Geophysical Research Letters*, *43*(7), 3280–3287. https://doi.org/10.1002/2016GL068210

494 Tejedor, A., Longjas, A., Edmonds, D. A., Zaliapin, I., Georgiou, T. T., Rinaldo, A., &
495 Foufoula-Georgiou, E. (2017). Entropy and optimality in river deltas. *Proceedings of the*
496 *National Academy of Sciences*, *114*(44), 11651–11656.
497 https://doi.org/10.1073/pnas.1708404114

498 Tognin, D., D'Alpaos, A., Marani, M., & Carniello, L. (2021). Marsh resilience to sea-level rise
499 reduced by storm-surge barriers in the Venice Lagoon. *Nature Geoscience*, *14*(12), 906–
500 911. https://doi.org/10.1038/s41561-021-00853-7

501 Wolinsky, M. A., Edmonds, D. A., Martin, J., & Paola, C. (2010). Delta allometry: Growth laws
502 for river deltas. *Geophysical Research Letters*, *37*(21), 1–6.
503 https://doi.org/10.1029/2010GL044592

504 Zoccarato, C., da Lio, C., Tosi, L., & Teatini, P. (2019). A coupled biomorpho-geomechanical
505 model of tidal marsh evolution. *Water Resources Research*, 2019WR024875.
506 https://doi.org/10.1029/2019WR024875

507

Supporting Information for "River delta morphotypes emerge from multiscale characterization of shorelines"

L. Vulis[1,2], A. Tejedor[1,3], H. Ma[1,4], J. H. Nienhuis[5], C. M. Broaddus[1,6], J. Brown[6], D. A. Edmonds[6], J. C. Rowland[2], E. Foufoula-Georgiou[1,7]

[1]Department of Civil and Environmental Engineering, University of California, Irvine, CA 92697

[2]Earth and Environmental Sciences Division, Los Alamos National Laboratory, Los Alamos, NM 87545

[3]Department of Science and Engineering, Sorbonne University Abu Dhabi, UAE

[4]State Key Laboratory of Hydroscience and Engineering, Tsinghua University, Beijing, China 100084

[5]Department of Physical Geography, Utrecht University, Utrecht, NL 3584CB

[6]Department of Earth and Atmospheric Sciences, Indiana University, Bloomington, IN 47405

[7]Department of Earth System Science, University of California, Irvine, CA 92697

Corresponding author: L. Vulis, Department of Civil and Environmental Engineering, University of California Irvine, Interdisciplinary Science and Engineering Building Room 3400, Irvine, CA 92612, USA. (lvulis@uci.edu).

,

Contents of this file

1. Text S1 to S3

2. Figures S1 to S4

Additional Supporting Information (Files uploaded separately)

1. Table S1. Delta extraction properties, metric values, and sediment fluxes

Introduction The Supporting Information for this manuscript includes a detailed description of the methods used for shoreline characterization, discussion on the use of the curvature operator for mapping shorelines to 1-D spatial-series, assessment of the morphometric classification sensitivity to the definition of the fine scale variance, and tabulated values of the morphometrics and sediment flux data.

,

Text S1. Extended Methodology

Shoreline Extraction

The Opening Angle Method (OAM; (Shaw et al., 2008)) was used to define the shorelines of the deltas under study. The OAM and related methods (Geleynse et al., 2012) are used in river mouth impacted coastlines where the traditional definition for a shoreline as the land water interface is not meaningful as the interface can extend far upstream of the actual river mouth.

To utilize the OAM, it is first necessary to generate a binary water mask of the subaerial extent of the delta. Water masks were generated from the Landsat-derived Global Surface Water (GSW) dataset, which provides 30-m spatial and monthly temporal resolution water masks from 1984 to 2018 and is available via Google Earth Engine (Pekel et al., 2016). An individual water mask was used for each delta. In order to account for missing data due to cloud cover and seasonal heterogeneity in water cover, water masks were generally obtained by thresholding the 1984 to 2018 occurrence product, which measures the fraction of time a pixel was covered by water from 1984 to 2018. In deltas with active shorelines e.g. the Danube or Wax Lake, the occurrence for a single representative year was used (Table S1), i.e. maps which measure the fraction of time a pixel was covered by water for a specific year. In the Arctic, snowmelt-driven floods from April to June lead to significant seasonal variability in inundation and apparent subaerial delta extent, therefore the June occurrence was used to identify maximum mouth extent (Vulis et al., 2021). When necessary, masks were manually cleaned to edit or remove features such as jetties or rice paddies, which are visible from contemporaneous satellite imagery

,

and the GSW has difficulty accounting for at its 30-m spatial resolution. Lastly, the OAM algorithm computes an opening angle on all water pixels that lie within the convex hull of the land in the water mask, which leads to unnecessary computations in channel sections upstream of the mouth which are entirely blocked by land. Therefore, these upstream sections were manually marked as land which decreased OAM runtime, as has been previously proposed (Baumgardner, 2015). The OAM was then run on the water mask corresponding to each delta. We made computational improvements to the OAM which significantly improved runtime, and have published this as an R package available via GitHub (https://github.com/lvulis/ROAM). A critical angle θ_c of 45° was then used to define the shoreline as an ordered set of coordinates $S_{45}^R : \{(x, y)_{45}\}$, although we found that the emergent shoreline classification does not change when using a critical angle θ_c of 50°. The shoreline defined in S_{45}^R only extends over the subaerial extent of the delta with start and end points of the shoreline defining the limits of the delta. The subaerial delta was visually outlined and compared with geologic maps where the extent was not clear from Landsat imagery. Note that in several deltas, non-depositional sections of the coastline were included in S_{45}^R, e.g. in valley confined systems such as the Dnieper and Don, and these were removed. Also note that the Missisippi Head of Passes, the Atchafayla, and Wax Lake deltas were all analyzed as separate systems due to their spatial independence in line with other studies (Galloway, 1975; Geleynse et al., 2012; Konkol et al., 2022; Knights et al., 2020).

Finally, to remove discretization artifacts on the shorelines which arise from being defined at the 30-m pixel scale, the raw shoreline in S_{45}^R was first smoothed using a Nadaraya-

,

Watson kernel smoother with a bandwidth of 180-meters (Strimas-Mackey, 2021) and then resampled at a 60-meter interval, resulting in the shoreline S_{45} used in the geometric and spectral analysis.

Macroscale – Shape

To measure the shape of the delta, a circle with parameters $\{(x_c, y_c), R_c\}$ was fit to S_{45} using least squares (Jammalamadaka & Sengupta, 2001). The shoreline may correspond only to a sector of a circle, which the least squares fit captures. The center of the circle (x_c, y_c) corresponds to the center of curvature and R_c the radius of curvature. Deltas with a center of curvature lying in the ocean are concave, while those with a center of curvature lying over land are convex. When R_c is significantly larger than the arc length L_C of the circular sector corresponding to the shoreline, the shoreline is essentially flat. That is, when the ratio $L_c/R_c = \varphi$, where φ is the angle of the sector, is smaller than a cutoff φ_{min}, the shoreline is flat. We found that a cutoff $\varphi_{min} = 2\pi/12 = 30°$ clearly separated flat from concave and convex deltas, i.e. if the shoreline corresponds to a circular sector with a radius at least 12 times its length, it is flat.

Mesoscale – Fraction of variance contributed by mouths

To measure the fraction of variance contributed by mouths (fM), first sections of S_{45} corresponding to mouths were identified by denoting which points in S_{45}^R are not a part of S_{90}^R, the shoreline corresponding to a critical angle of $\theta_c = 90°$, i.e. $M_{45}^R = \{(x_i, y_i) | (x_i, y_i) \in S_{45}^R$ and $\notin S_{90}^R\}$. This is because OAM-defined shorelines using different critical angles do not overlap within local concavities (e.g. mouths or embayments). This definition may include embayments such as lagoons sheltered by spits, therefore M_{45}^R was manually inspected and

,

cleaned to represent only mouths. Lastly, the same smoothing procedure used to transform S_{45}^R to S_{45} was used to smooth M_{45}^R and produce M_{45}, which identifies the set of points in the smoothed shoreline as mouths.

Then to measure what fraction of variability in S_{45} is contributed by M_{45} we used wavelet analysis to locally estimate the variance in shoreline structure at multiple scales (Kumar & Foufoula-Georgiou, 1994). For the wavelet analysis a univariate series representing the shoreline was produced as the distance d_c from every point in S_{45} to the center of curvature (x_c, y_c), defining a signal $d_c(l)$, where l is the distance along the shoreline. For convex deltas, the mouths show up as minima, which can be seen in the Mahakam Delta (Fig. 2). We found that this mapping of the shoreline to a univariate series is preferable to approaches such as extracting the local curvature series, which is effectively a high-pass filter removing large scale features and is sensitive to discretization, see Text S3. Note that mouth widths are typically non-uniform within a delta, resulting in multiscale variability in the $d_c(l)$ signal, supporting the use of localized analysis of variance in the spatial domain. Then, the wavelet transform of $d_c(l)$ was computed using the Morlet wavelet, which has optimal time-frequency localization, with a central frequency of 6 rad/s (Kumar & Foufoula-Georgiou, 1994). The wavelet coefficients are given by $\Psi_{k,l}$ at a wavenumber (spatial frequency) k and location l along the shoreline, and are used to estimate the power, $\Psi_{k,l}^2$ (Fig. S2). Finally, the fM is defined as the ratio of the integrated wavelet power for all scales over coefficients corresponding to the mouths, $\Psi_{k,l\in M}$ over the total power (i.e. variance) of the signal (Eqn. 1), where L is the length of the shoreline and k_{min} and k_{max} are the minimum and maximum wavenumbers, respectively. Note

,

that typically, wavelet coefficients inside the cone of influence (COI) are excluded from the computation of the variance as they are impacted by edge effects. However, in some deltas the mouths may contain very large features, sometimes spanning over one third of the length of the signal, therefore for all deltas these coefficients were included for more robust estimation of the relative energy in these locations.

$$fM = \int_{k_{min}}^{k_{max}} \int_0^L \Psi^2_{k,l\in M} dldk / \int_{k_{min}}^{k_{max}} \int_0^L \Psi^2_{k,l} dldk. \quad (1)$$

Microscale – Gini-Corrected Fine Scale Variance

Lastly the wavelet transform (Kumar & Foufoula-Georgiou, 1994) was used to estimate the variance at fine scales, i.e. from 300 to 1000 meters (Eqn. 2). Note that here edge effects from the COI can significantly influence the estimated amount of energy at the scales of the features under study, therefore coefficients inside the COI are excluded and the power at each wavenumber k is normalized by the number of points at that frequency, N_k. The sensitivity of the lower bound of 1000 meters was evaluated and no significant changes in the classification were found (Fig. S1).

$$FSV_{1000} = \frac{1}{N_k} \int_{1/1000}^{1/300} \int_0^L \Psi^2_{k,l} dldk. \quad (2)$$

Although two systems may have the same variance at fine scales, one may lack structural variability (i.e. correspond to white noise), while another may have peaks or increased variability at distinct scales. To account for this structured variability, the power spectral density (PSD) of the actual shoreline spatial series is compared to a white noise series with equivalent variance. Specifically, a spectral Gini coefficient g, which measures the total deviation of the cumulative PSD ($cPSD$) from the $cPSD$ of white noise is computed over

,

the fine scales, and used as a multiplier to the FSV_{1000}, defining the $gFSV = g * FSV_{1000}$. This multiplier is low when shoreline variability is similar to white noise, and high when shoreline variability has defined structures (i.e. peaks or higher energy at finer or coarser scales), and helps to separate deltas with similar FSV_{1000} but distinct modes of variability (see Text S2 for details).

All analyses were performed in R using open source geospatial, statistical, and spectral analyses packages (Strimas-Mackey, 2021; Pebesma, 2018, 2021; Pau et al., 2010; Morgan-Wall, 2021; Aybar, 2022; Gouhier et al., 2021).

Sediment Flux Data

Sediment fluxes for every delta were obtained from version 3 of the Nienhuis et al. (2020) database, which used the WBMSed hydrologic model forced with 1981 to 2010 hydroclimate and assuming no human intervention of landscape properties to estimate riverine sediment fluxes, Q_R, (Cohen et al., 2013), angular wave climate data from WaveWatch 3.0 (Chawla et al., 2013) averaged from 1979 to 2009 to estimate wave sediment fluxes, Q_W, and tidal constituents from TXPOv8 inverted from satellite altimetry measurements from 1992 to 2006 (Egbert & Erofeeva, 2002) to estimate tidal sediment fluxes, Q_T. To reduce uncertainty in tidal amplitude estimates associated with the delta outlet location being located too far upstream of the coastline in the global delta database, for all deltas tidal amplitudes from the TXPO grid were obtained at the OAM shoreline extracted at a critical angle 90°. This only resulted in a difference of more than 5 cm for 9 out of 54 deltas, all with significantly widened mouths.

,

Sediment flux data represents a delta-wide value, see (Nienhuis et al., 2020) and references therein for details. For every delta, the relative sediment flux r_x, where x represents either the river, wave, or tide component is defined as:

$$r_x = \frac{Q_x}{Q_R + Q_T + Q_W}. \tag{3}$$

,

Text S2. Spectral Gini Coefficient Definition In order to help separate wave-influenced deltas which are smooth and lack distinct features in the fine scale ranges from the river and tide influenced deltas which contain structure at fine scales, we adjusted the finescale variance by a spectral gini coefficient. To define the spectral gini coefficient and interpert this adjustment, first consider the wavelet-estimated power spectral density, given by Eqn. 4,

$$PSD(k) = \frac{1}{N_k} \int_0^L \Psi_{k,l}^2 dl, \tag{4}$$

where l is the location and k the wavenumber (scale). The spectral variance SV for a range of wavenumbers (scales) k_0 to k_1 is found by integrating with respect to k:

$$SV = \int_{k_0}^{k_1} PSD(k) dk. \tag{5}$$

In general, two signals may have identical SV for a given range of scales but distinct structure. For example, white noise, which by definition has a constant PSD, i.e. $PSD_{WN} = P$, and lacks any structural variability, may have the same SV as a signal with structured variability. To measure the deviation from white noise, consider the normalized PSD, $PSD^*(k)$, given in (Eqn. 6). $PSD^*(k)$ is analogous to a probability density function (PDF), where the integral over the support (i.e. from k_0 to k_1) is 1.

$$PSD^*(k) = \frac{PSD(k)}{SV}. \tag{6}$$

White noise has a uniform spectrum (i.e. flat PSD), while the PSD of another signal may be distributed heterogeneously over the range of wavenumbers (Fig. S2). We then consider the normalized cumulative power spectral density, $cPSD^*(k)$, where k can take

,

on any value up to k_1:

$$cPSD^*(k) = \int_{k_0}^{k} PSD^*(u)du. \tag{7}$$

White noise has a linear $cPSD^*$, while the shoreline $cPSD^*$ is skewed towards relatively coarser scales for $k_0 = \frac{1}{1000}$ m^{-1} and $k_1 = \frac{1}{300}$ m^{-1} (Fig. S2). For these skewed distributions, a natural measure of the deviation from a uniform distribution is the Gini Coefficient, g, which measures the area between the $cPSD^*(k)$ of white noise, $cPSD^*_{WN}(k)$, and the $cPSD^*(k)$ of the shoreline, normalized by the area under the curve of $cPSD^*_{WN}(k)$. As these distribution functions represent spectra this is a spectral Gini Coefficient.

$$g = \frac{\int_{k_0}^{k_1} (cPSD^*_{WN}(k) - cPSD^*(k))dk}{\int_{k_0}^{k_1} cPSD^*_{WN}(k)dk}. \tag{8}$$

The coefficient g increases towards a maximum value of 1 as the PSD is more heterogeneous and approaches zero as the PSD approximates white noise. This coefficient is used as a multiplier to the FSV, computed from $k_0 = \frac{1}{1000}$ m^{-1} to $k_1 = \frac{1}{300}$ m^{-1}, of the shoreline spectra, accounting for the heterogeneous distribution of variance among scales indicative of distinct scale-dependent features (Fig. S2).

,

Text S3. Unsuitability of curvature mapping for shoreline characterization

A common technique to quantitatively analyze meandering rivers is to map the 2D curve corresponding to the channel centerline to a 1D spatial-series represented by its curvature, e.g. (Schwenk et al., 2015), which could also be applied to delta shorelines to perform wavelet analysis. However, for the problem of shoreline characterization we found that the high-pass filter properties of the curvature operator make it unsuitable for extraction of large scale patterns such as channel mouths using spectral analysis. A synthetic example using sinusoids is given to demonstrate these high-pass filter properties. Consider two sinusoids of differing wavenumber with random additive error, $z_1(s) = 5\sin(s) + \mathcal{N}(0, .5)$ and $z_2(s) = 20\sin(\frac{s}{2\pi}) + \mathcal{N}(0,\ 2)$, along with their sum $z_3(s) = z_2(s) + z_1(s)$ (Fig. S3). The sinusoids represent spatial-series with s being some distance along the shoreline, and are sampled with spatial step $\Delta s = 1$. To analyze the oscillations, the Fourier transform $\hat{z}(k)$ with wavenumber k is taken, with the power spectral density of each signal given in the right panel of (Fig. S3). The additive signal z_3 has clearly defined peaks at $k = (2\pi)^{-1}$ and $k = (2\pi)^{-2}$.

In the case where the functional relationship between z and s is not known, we may want to map the set of coordinates of each $\{(s, z)_i\}$ to a univariate series to employ spectral analysis to characterize the curve. One such common mapping is defining the local curvature κ. For an ordered set of coordinates $\{(x, y)_i\}$ constituting a 2D planar curve, a stable and smooth estimator of the local curvature $\kappa = 1/R$ is given in (Schwenk et al., 2015):

,

$$R = \frac{1}{2}\frac{\sqrt{(\mathbf{a_x^2}+\mathbf{a_y^2})(\mathbf{b_x^2}+\mathbf{b_y^2})(\mathbf{c_x^2}+\mathbf{c_y^2})}}{(\mathbf{a_y b_x}-\mathbf{a_x b_y})}, \tag{9}$$

where $\mathbf{a_x} = x_i - x_{i-1}$, $\mathbf{b_x} = x_{i+1} - x_{i-1}$,$\mathbf{c_x} = x_{i+1} - x_i$. This definition and related curvature operators given in (Schwenk et al., 2015) clearly depend on the sampling resolution of the 2-D planar curve.

The curvature is computed for each curve given by the $\{(s, z)\}$ coordinate pairs to define a univariate series $\kappa(l)$, where l is the distance along the curve (Fig. S4). The noise present in the original signals is amplified by taking local differences and results in the large variation seen in κ_2 and κ_3. The corresponding power spectral density shows that for the high wavenumber series, κ_1, the curvature mapping still captures the wavenumber observed in z_1, but κ_2 and κ_3 have no power near the real wavenumber of $(2\pi)^{-2}$. This is because taking finite differences to compute the curvature filters out the low wavenumber signal.

The sensitivity or ability to capture the low wavenumber signal likely depends on the ratio of the sampling wavenumber $k_s = \Delta s^{-1}$ to the wavenumber of interest k_u, k_s/k_u. By the Nyquist theorem, this ratio must be at least 2 to resolve k_u. When the ratio approaches 2 from a larger value, noise may not be amplified by the curvature transformation, but when it is much larger than 2 noise is amplified. Some value sufficiently optimal to capture k_u using the curvature transformation may exist. However, mouth widths are not constant on deltas and can vary at least by a factor of 2, therefore k_u can vary significantly, so a k_s optimal for the narrowest mouth will amplify noise in the remaining, larger mouths. Moreover, a sufficiently high k_s to capture mouths would filter out information at low

,

wavenumbers, e.g. large scale features such as deltaic lobes. For these reasons the mapping of curvature is not suitable for the problem of shoreline characterization.

References

Aybar, C. (2022). rgee: R bindings for calling the 'earth engine' api [Computer software manual]. Retrieved from `https://CRAN.R-project.org/package=rgee` (R package version 1.1.3)

Baumgardner, S. E. (2015). *Quantifying galloway: Fluvial, tidal and wave influence on experimental and field deltas* (Unpublished doctoral dissertation). University of Minnesota.

Chawla, A., Spindler, D. M., & Tolman, H. L. (2013). Validation of a thirty year wave hindcast using the climate forecast system reanalysis winds. *Ocean Modelling*, *70*, 189–206.

Cohen, S., Kettner, A. J., Syvitski, J., & Fekete, B. M. (2013). Wbmsed, a distributed global-scale riverine sediment flux model: Model description and validation. *Computers & Geosciences*, *53*, 80–93.

Egbert, G. D., & Erofeeva, S. Y. (2002). Efficient inverse modeling of barotropic ocean tides. *Journal of Atmospheric and Oceanic technology*, *19*(2), 183–204.

Galloway, W. E. (1975). Process framework for describing the morphologic and stratigraphic evolution of deltaic depositional system. In *Deltas: Models for exploration* (pp. 87–98). Houston Geological Society.

Geleynse, N., Voller, V., Paola, C., & Ganti, V. (2012). Characterization of river delta shorelines. *Geophysical research letters*, *39*(17).

,

Gouhier, T. C., Grinsted, A., & Simko, V. (2021). R package biwavelet: Conduct univariate and bivariate wavelet analyses [Computer software manual]. Retrieved from `https://github.com/tgouhier/biwavelet` ((Version 0.20.21))

Jammalamadaka, S. R., & Sengupta, A. (2001). *Topics in circular statistics* (Vol. 5). world scientific.

Knights, D., Sawyer, A. H., Barnes, R. T., Piliouras, A., Schwenk, J., Edmonds, D. A., & Brown, A. M. (2020). Nitrate removal across ecogeomorphic zones in wax lake delta, louisiana (usa). *Water Resources Research*, *56*(8), e2019WR026867.

Konkol, A., Schwenk, J., Katifori, E., & Shaw, J. B. (2022). Interplay of river and tidal forcings promotes loops in coastal channel networks. *Geophysical Research Letters*, *49*.

Kumar, P., & Foufoula-Georgiou, E. (1994). Wavelet analysis in geophysics: An introduction. *Wavelets in geophysics*, *4*, 1–43.

Morgan-Wall, T. (2021). rayshader: Create maps and visualize data in 2d and 3d [Computer software manual]. Retrieved from `https://CRAN.R-project.org/package=rayshader` (R package version 0.24.10)

Nienhuis, J. H., Ashton, A. D., Edmonds, D. A., Hoitink, A., Kettner, A. J., Rowland, J. C., & Törnqvist, T. E. (2020). Global-scale human impact on delta morphology has led to net land area gain. *Nature*, *577*(7791), 514–518.

Pau, G., Fuchs, F., Sklyar, O., Boutros, M., & Huber, W. (2010). Ebimage—an r package for image processing with applications to cellular phenotypes. *Bioinformatics*, *26*(7), 979–981. doi: 10.1093/bioinformatics/btq046

,

Pebesma, E. (2018). Simple Features for R: Standardized Support for Spatial Vector Data. *The R Journal*, *10*(1), 439–446. Retrieved from https://doi.org/10.32614/RJ-2018-009 doi: 10.32614/RJ-2018-009

Pebesma, E. (2021). stars: Spatiotemporal arrays, raster and vector data cubes [Computer software manual]. Retrieved from https://CRAN.R-project.org/package=stars (R package version 0.5-5)

Pekel, J.-F., Cottam, A., Gorelick, N., & Belward, A. S. (2016). High-resolution mapping of global surface water and its long-term changes. *Nature*, *540*(7633), 418–422.

Schwenk, J., Lanzoni, S., & Foufoula-Georgiou, E. (2015). The life of a meander bend: Connecting shape and dynamics via analysis of a numerical model. *Journal of Geophysical Research: Earth Surface*, *120*(4), 690–710.

Shaw, J. B., Wolinsky, M. A., Paola, C., & Voller, V. R. (2008). An image-based method for shoreline mapping on complex coasts. *Geophysical Research Letters*, *35*(12).

Strimas-Mackey, M. (2021). smoothr: Smooth and tidy spatial features [Computer software manual]. Retrieved from https://CRAN.R-project.org/package=smoothr (R package version 0.2.2)

Vulis, L., Tejedor, A., Zaliapin, I., Rowland, J. C., & Foufoula-Georgiou, E. (2021). Climate signatures on lake and wetland size distributions in arctic deltas. *Geophysical Research Letters*, *48*(20), e2021GL094437.

,

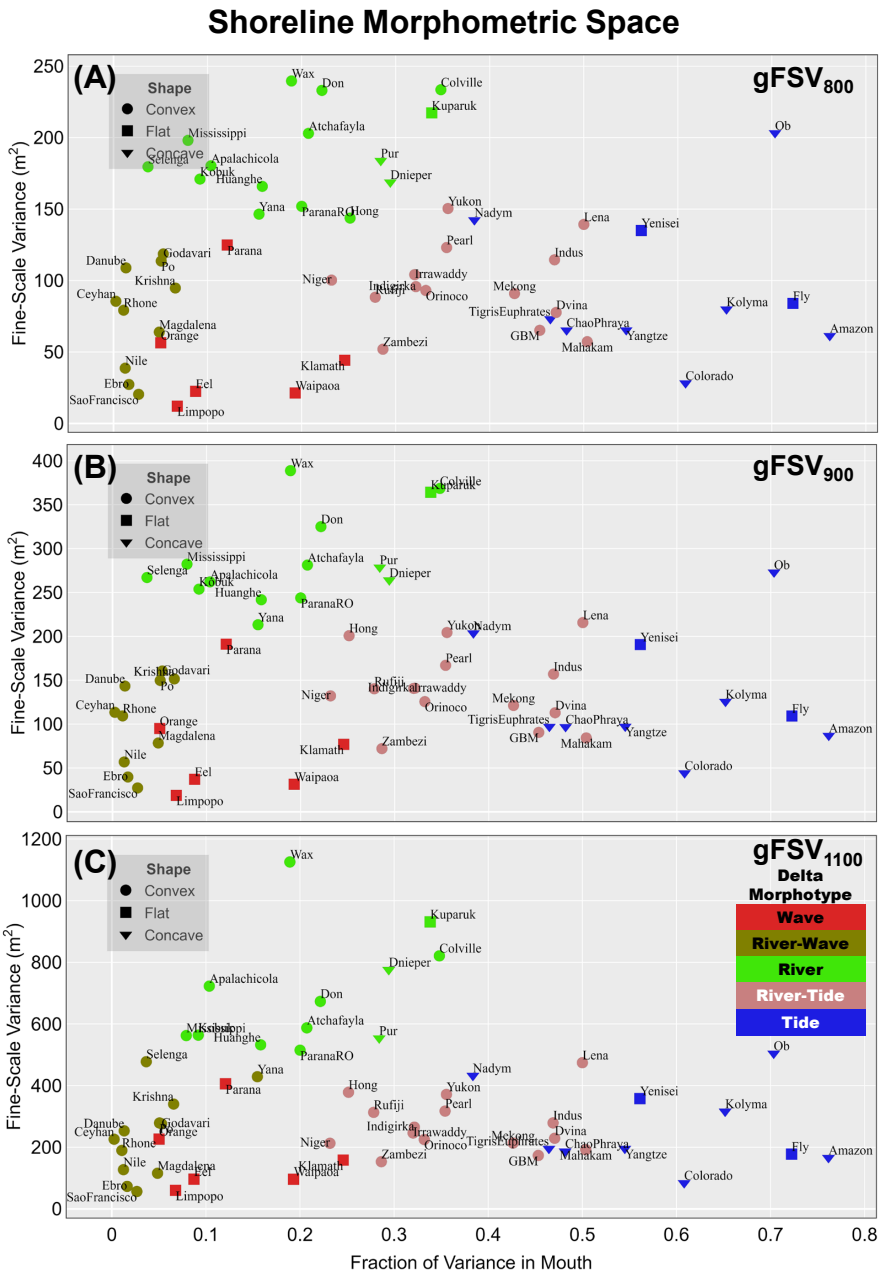

Figure S1. Insensitivity of the emergent classes to the upper bound of the finescale variance. There is almost no discernible difference in the deltas belonging to each emergent morphotype when adjusting the upper wavelength of the Gini-corrected Fine Scale Variance ($gFSV$) between 800 m to 1100 m. Only the Selenga and Yana switch from the river morphotype to river-wave morphotype for an upper wavelength of 1100 m, but lay on the boundary of the two classes.

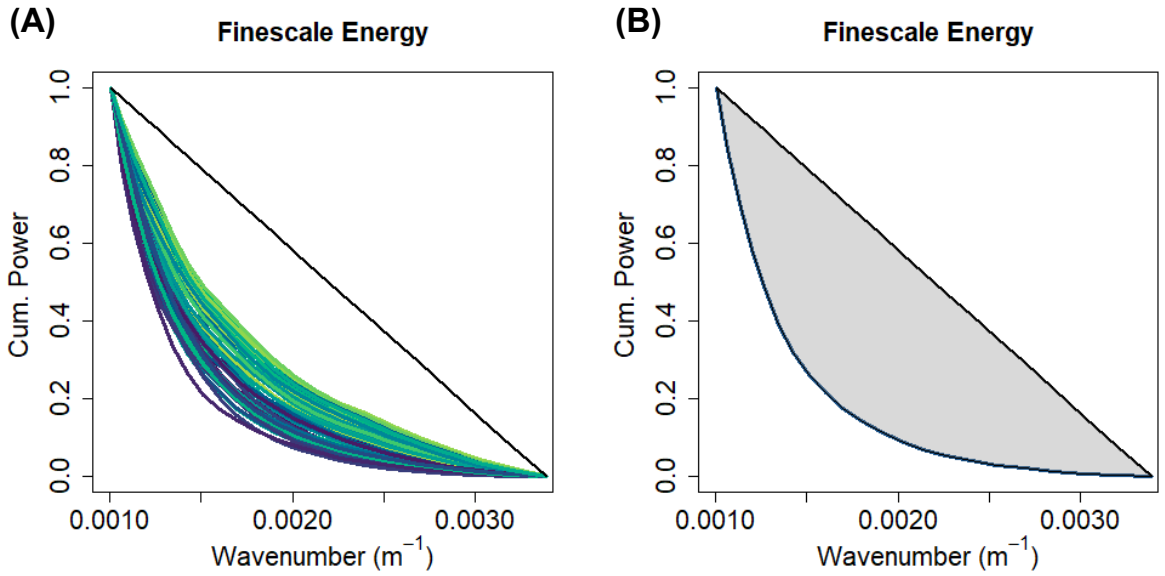

Figure S2. Cumulative Power Spectral Density ($cPSD^*$) of the shoreline signals. (A) The $cPSD^*$ curves of the 54 analyzed delta shorelines, each normalized to have a value of one over the fine scales. The straight black line is $cPSD^*_{WN}$ and overlaps for each delta due to the normalization to have unit power. (B) Example of the deviation between an arbitrarily selected real shoreline and white noise with equivalent energy. The Gini Coefficient (g) is the area between the two curves normalized by the area under the white noise.

,

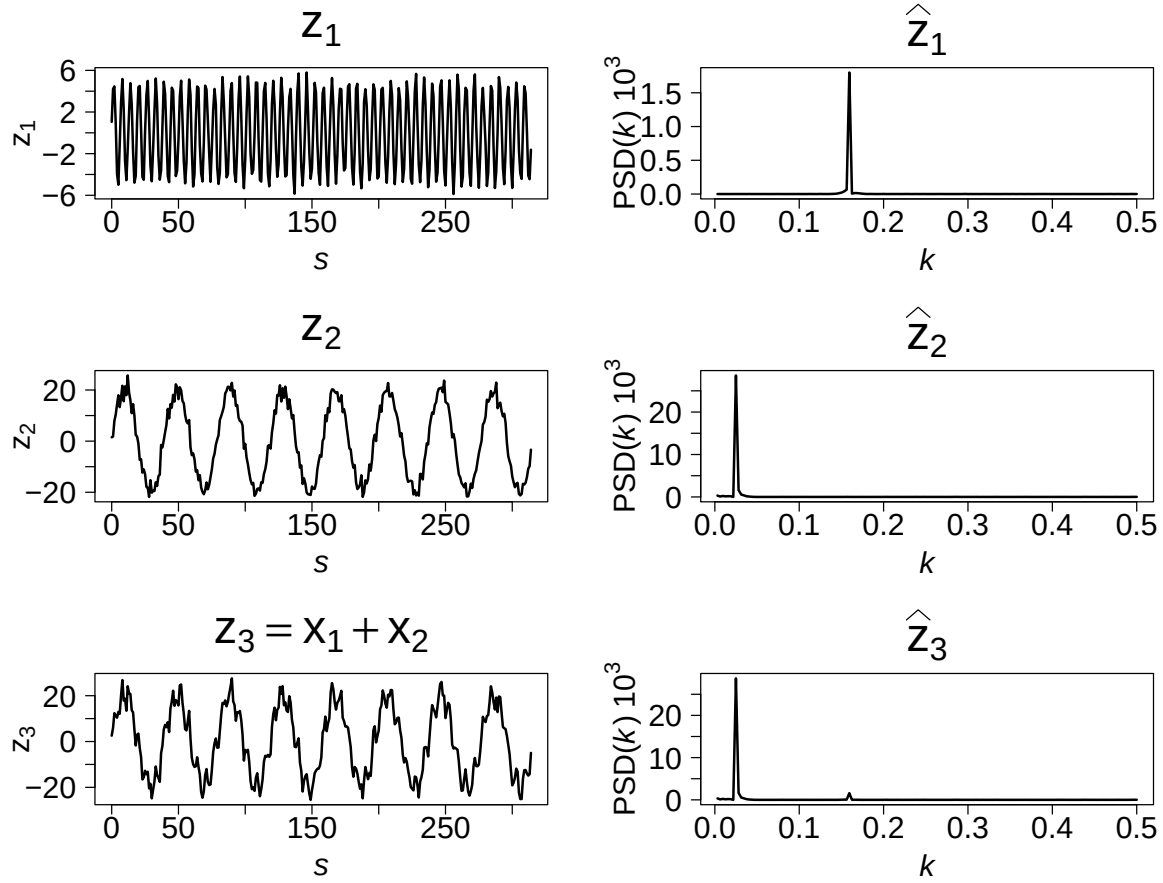

Figure S3. Synthetic sinusoids and their corresponding power spectral density.

,

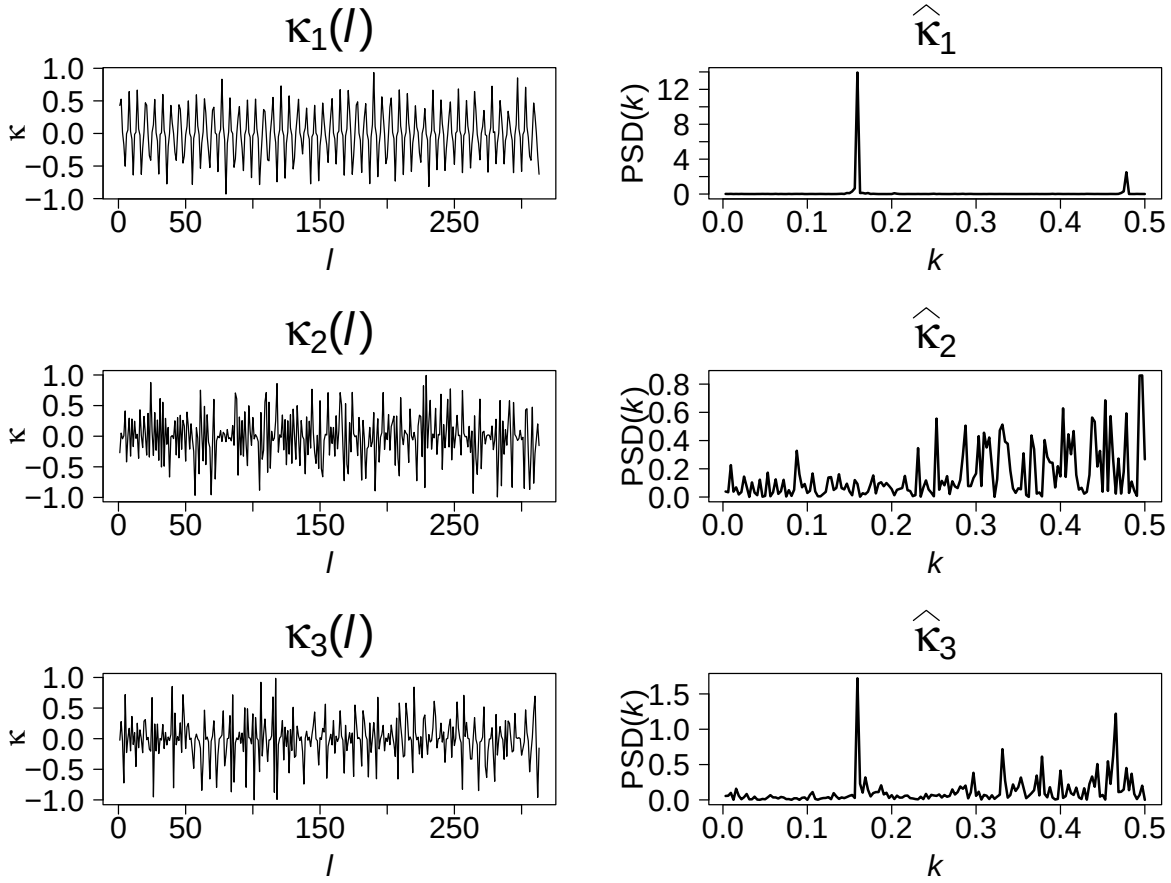

Figure S4. Result of the curvature operator on sinusoids. The sinusoids from Fig. S3 transformed to curvature spatial-series using Equation (9). Note that κ_2 and κ_3 fail to capture the low frequency signal present in z_2 and z_3.

,